Detonation Front Curvature Measurements and Aquarium Tests of Tritonal Variants

Helen Dorsett and Matthew D. Cliff

Weapons Systems Division
Defence Science and Technology Organisation

DSTO-TR-1411

ABSTRACT

'Alex', an ultrafine aluminium powder, burns more rapidly than conventional aluminium powders in energetic materials. In TNT-based formulations, the increased rate of energy release leads to higher detonation pressures and velocities. In order to determine the rate of Alex combustion in solid explosives, and to further assess its effects on the detonation properties of TNT formulations, aquarium tests and detonation front curvature tests were performed on Tritonal variants. The aquarium tests definitively show that Alex combustion in detonating Tritonal is significantly faster than that of Cap45a, the conventional aluminium powder used for military explosives. Additional pressure and velocity measurements from the aquarium tests agree with previous experiments. The results of detonation front measurements were less conclusive, but show qualitive trends that support existing data.

Report Documentation Page

Form Approved
OMB No. 0704-0188

1. REPORT DATE	2. REPORT TYPE	3. DATES COVERED
01 APR 2003	**N/A**	**-**

4. TITLE AND SUBTITLE	5a. CONTRACT NUMBER
Detonation Front Curvature Measurements and Aquarium Tests of Tritonal Variants	5b. GRANT NUMBER
	5c. PROGRAM ELEMENT NUMBER
6. AUTHOR(S)	5d. PROJECT NUMBER
	5e. TASK NUMBER
	5f. WORK UNIT NUMBER
7. PERFORMING ORGANIZATION NAME(S) AND ADDRESS(ES) **Weapons Systems Division Defence Science and Technology Organisation**	8. PERFORMING ORGANIZATION REPORT NUMBER
9. SPONSORING/MONITORING AGENCY NAME(S) AND ADDRESS(ES)	10. SPONSOR/MONITOR'S ACRONYM(S)
	11. SPONSOR/MONITOR'S REPORT NUMBER(S)

12. DISTRIBUTION/AVAILABILITY STATEMENT
Approved for public release, distribution unlimited

13. SUPPLEMENTARY NOTES
See also ADM001524. DSTO-TR-1411, The original document contains color images.

14. ABSTRACT

15. SUBJECT TERMS

16. SECURITY CLASSIFICATION OF:			17. LIMITATION OF ABSTRACT	18. NUMBER OF PAGES	19a. NAME OF RESPONSIBLE PERSON
a. REPORT	b. ABSTRACT	c. THIS PAGE			
unclassified	**unclassified**	**unclassified**	**UU**	**49**	

Standard Form 298 (Rev. 8-98)
Prescribed by ANSI Std Z39-18

Published by

DSTO Systems Sciences Laboratory
PO Box 1500
Edinburgh South Australia 5111 Australia

Telephone: (08) 8259 5555
Fax: (08) 8259 6567

AR-012-729
April 2003

APPROVED FOR PUBLIC RELEASE

Detonation Front Curvature Measurements and Aquarium Tests of Tritonal Variants

Executive Summary

'Alex'[1], an ultrafine aluminium powder, burns more rapidly than conventional aluminium powders in energetic materials, and has been shown to enhance the detonation performance of various formulations of aluminised TNT, also known as 'Tritonal'[2]. This performance enhancement was evidenced by an increase in detonation velocity, measured by streak photography and piezoelectric arrays, and a relative increase in detonation pressure as measured from the dent depths of witness plates. In order to further elucidate the influence of Alex upon Tritonal detonation, two additional experiments were performed to complement these standard measurements, namely, aquarium tests and detonation front curvature measurements.

The aquarium test is a simple, well-known technique that involves taking high-speed photographs of an underwater detonation. As in air, the velocity of the detonation front can be determined from streak photography. The pressure of the detonation front can also be estimated from formation of the shock wave in water. Information on late-time chemical reactions that follow the detonation front may be obtained from the shape of the ensueing 'bubble' of gaseous detonation products. Hence, if the faster combustion rate of Alex significantly influences bubble formation (analogous to the 'blast' following detonation in air), these effects will be immediately apparent from aquarium test photographs.

Apart from these standard applications, the aquarium tests performed at DSTO serve yet another purpose. From previous tests on aluminised underwater explosives, it was discovered that the high-speed camera used in the High Explosives Firing Chambers (HEFC) facility can record light emitted from the burning aluminium, and can therefore be used to measure the rate of aluminium combustion. These experiments on Tritonal variants represent the first time aquarium tests have been used to measure rates of aluminium combustion in aluminised explosives, and the results provide vivid, definitive evidence that Alex burns faster than Cap45a (a conventional aluminium) in Tritonal formulations. Aquarium tests are also one of only a few experiments capable of measuring any type of chemical reaction rate in solid explosives during (and immediately following) detonation. As they are relatively simple and inexpensive experiments, it is reasonable to expect that aquarium tests could also be used to measure combustion rates of other solid fuels in energetic formulations.

---

[1] The trade name Alex® (Argonide Corporation) is an acronym derived from 'electro-exploded aluminium,' the process of production that involves driving large currents through aluminium wire (under an inert atmosphere) until it explodes into fine particles.

[2] 'Tritonal' is the common name for a formulation consisting of 80% TNT and 20% aluminium.

The Alex-induced performance enhancement of Tritonal is most pronounced for ‘non-ideal’ detonation. Hence, detonation front curvature measurements were performed to further investigate how Alex combustion affects ‘non-ideal’ detonation. Under non-ideal conditions, the detonation front is subject to energy losses which degrade performance and exaggerate effects induced by the size and shape of the charge. In small cylindrical sticks of explosives, non-ideal detonation is manifested by the appearance of a curved detonation front, which arises from energy losses at the edge of the cylinder that cause the sides of the detonation front to lag behind the center. If the diameter of the cylinder is reduced (or the detonation becomes more ‘non-ideal’), the energy losses increase and the detonation front curvature becomes more pronounced. The faster combustion rate of Alex may compensate for these energy losses, leading to a reduction in detonation front curvature compared with conventional Tritonal.

Like the aquarium tests, the detonation front curvature measurements are relatively simple experiments to perform, with the main requirement being high-speed photography of the detonation front as it exits the charge. The results of these experiments were less conclusive than those of the aquarium tests, however, many of the observed inconsistencies may be attributed to unfamiliarity with the technique and casting irregularities within the charges. In light of continuing development of explosives that are “tailor-made” to specific applications, this simple, inexpensive and non-intrusive technique may prove a valuable asset for on-site assessment of small explosive charges in the High Explosive Firing Chambers at DSTO Edinburgh.

Authors

Helen Dorsett
Maritime Operations Division

Helen Dorsett obtained a doctorate in physical chemistry from the University of Maryland (USA), and joined WSD in 1998. Her work in the Explosives Group included quantum chemical modelling of energetic molecules and small-scale testing of underwater explosives. She is now a member of the Amphibious and Mine Warfare Operations Group within the Maritime Operations Division at DSTO-Sydney, modelling mine clearance operations.

Matthew D. Cliff
Weapons Systems Division

Matthew Cliff completed his Honours degree at Deakin University in 1991 and his PhD in organic chemistry at the University of Woolongong in 1995. He joined AMRL in 1996 and has worked on a range of tasks including new explosives synthesis, composition formulation and evaluation, IM testing and weapon performance T&E, and research into melt-castable Insensitive Munition fills and reactive metals for enhanced blast warheads. In 1998/1999 he was attached to the Defence Evaluation and Research Agency, Fort Halstead in the UK, and in 2002 he joined the editorial board of the Journal of Energetic Materials. He is currently serving as Staff Officer Science at Army Land Headquarters, NSW.

Contents

List of Acronyms

ADN	ammonium dintramide - an oxidizer and low-order explosive
Al	aluminium
Alex®	electro-exploded aluminium powder, with particles sizes of 100-200nm
ANFO	ammonium nitrate/fuel oil – an explosive formulation used in mining applications
AP	ammonium perchlorate - an oxidizer and low-order explosive
BTNNA	bis(2,2,2-trinitroethyl)nitramine - a high explosive
Cap45a	commercial grade aluminium powder, with particles sizes of 10-20μm
CCD	charge-coupled device – the electronic sensors of a digital camera
CL-20	hexanitrohexazaisowurtzitane - high explosive
HEFC	High Explosives Firing Chamber
HMX	cyclotetramethylenetetranitramine - a high explosive
NM	nitromethane – a high explosive
PMMA	polymethyl methacrylate – a plastic (*i.e.*, “Perspex ™”)
P_{CJ}	detonation or Chapman-Jouguet pressure
RDX	cyclotrimethylenetrinitramine – a high explosive
TATB	triaminotrinitrobenzene – an insensitive high explosive subject to non-ideal detonation at small charge sizes
TNT	trinitrotoluene – a high explosive
VoD	velocity of detonation

1. Introduction

Aluminium powders are commonly added to explosive formulations to enhance late-time (post-detonation) effects such as air blast or, for underwater explosives, bubble energies. Compared to the chemical reactions of the high explosive ingredients (*eg*., TNT or RDX) that occur in the detonation front, combustion of conventional aluminium powders is a relatively slow process. Hence, it is generally assumed that most of the aluminium remains inert within the detonation front, and that the energy it releases does not contribute to properties such as velocity of detonation (VoD) or detonation pressure (P_{CJ}).

Conventional weapons grade aluminium powders such as Cap45a have particle sizes of approximately 10-20 microns (see Fig. 1). However, sub-micron sized aluminium powders have recently become available; one such ultrafine powder, 'Alex®' consists of spherical particles typically 100-200 nanometres in diameter [1]. The small particle size of Alex® leads to a significantly higher rate of combustion [2] and a shorter ignition delay [3]. Replacing conventional aluminium with Alex® produces dramatic improvements in the burn performance of propellants [1-4], and enhances the detonation properties of aluminised explosive formulations containing ammonium dinitramide [5] and TNT [6]. However, similar treatment of formulations containing RDX or HMX leads to unchanged or even diminished performance [4-7]. Hence, there is as yet no clear general model of how combustion of ultrafine aluminium can influence the detonation properties of solid explosives.

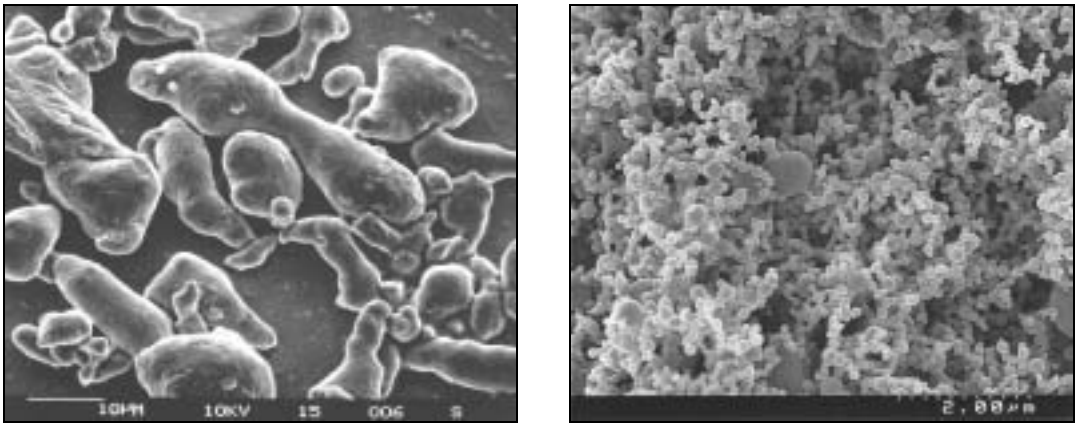

Figure 1. SEM photographs of CAP45a (left) and Alex® (right). Note differences in scale.

To further elucidate the effects of Alex® upon the detonation properties of solid explosives, two series of detonation experiments - aquarium tests and detonation front curvature measurements – were performed on Tritonal variants to complement earlier dent test (detonation pressure) and velocity of detonation measurements carried out at DSTO [6]. The aquarium tests were extremely successful, and the results were presented at several general science [8] and defence science [9] fora. The detonation front curvature measurements were less conclusive, but display qualitative trends that support existing data.

Since both of these experiments add capability to on-site explosives testing at the HEFC facilities in Edinburgh, they are each described in detail in this report, along with recommendations and suggested improvements. The experimental results are presented in light of the unique properties of Alex®, and the report concludes with a discussion of the possible mechanisms that underlie the observed Alex®-induced performance enhancement of Tritonal.

In order to assist future modelling efforts for these experiments, all images have been saved in tagged image file format (i.e., *.TIF files) on a CD-ROM that accompanies this report. Image analysis and velocity of detonation calculations performed by the authors is also provided on the CD-ROM as MS Excel worksheets. Information regarding the interpretation and calibration of aquarium test photographs is given in Appendix A.

2. The Explosive Charges

The Alex®-induced performance enhancement is most pronounced for ‘non-ideal’ detonation of Tritonal. Details of these effects will be discussed in the conclusions of this report, however, it is important to note now that under ‘non-ideal’ conditions, the detonation of an explosive charge will depend strongly upon its size and shape and - particularly for TNT-based formulations - how it is cast. For instance, cylindrical sticks of ‘cast clear’ TNT will fail to detonate if the charge diameter is smaller than 32mm, whereas the failure diameter of ‘cast cloudy’ TNT ranges from 22 - 25mm [10].

TNT and Tritonal charges for both experiments were cast as either 1” (25.4mm) or 2” (50.8mm) diameter cylinders, with lengths of 200mm (aquarium tests) or 250mm (curvature measurements). Only 1” charges of ‘cast clear’ TNT charges were fabricated, and these served simply as benchmarks since, as expected, they failed to detonate. VoD measurements of the 1” ‘cast-cloudy’ TNT charges show a failing detonation, also in agreement with previous results. Examples of the charges are shown in Fig. 2.

The conventional aluminium used in this study - Cap45a - was sourced from Comalco Aluminium Powders (Australia). Alex® was obtained from Argonide Corporation (USA). All Tritonal charges were cast from the same batch of TNT and of the respective aluminium powders.

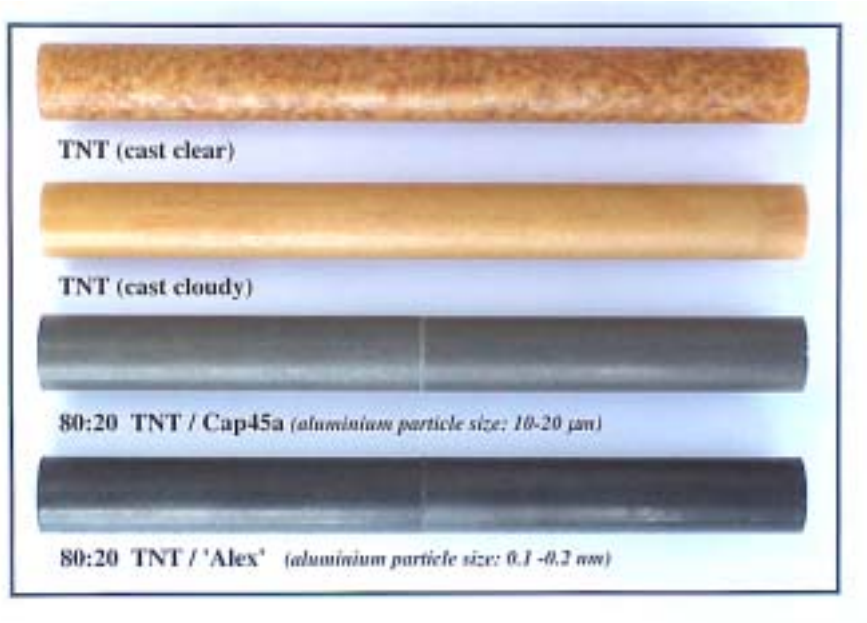

Figure 2. Explosives used in the aquarium tests and the detonation curvature measurements. The samples shown are cylinders 1" (25.4mm) in diameter and 250mm long. Some Tritonal charges were cast in two pieces and then glued together.

To reduce sedimentation of the aluminium particles due to the slow rate of TNT solidification, the 250mm Tritonal charges were cast in two pieces, then glued together with Araldite® epoxy just prior to the experiment. The Alex®-Tritonal charges proved to be quite brittle and broke easily; the edges of broken charges were re-machined to provide a smooth surface for reattachment. The glued joints had no apparent effect upon the progress of the detonation.

3. Aquarium Tests

As suggested by the name, aquarium tests are typically used to study underwater detonations, particularly early-time formation of the water shock wave and the gas bubble of detonation products. This is achieved through high-speed photography of the detonation as it proceeds. If the detonation front is sufficiently bright, the velocity of the detonation can be obtained from streak photography. The detonation pressure is estimated from the interaction of the detonation shock front with the water. Information regarding late-time chemical reactions that occur soon after the detonation front may be obtained from the shape of the ensuing 'bubble' of gaseous detonation products. Aquarium tests also provide a rigorous assessment of detonation models for the explosive since, aside from some slight optical distortions, the frame images can be compared directly to hydrocode simulations. A good discussion of these measurements is provided in Craig *et. al.* [11] and Goldstein and Johnson [12].

'Standard' aquarium tests can provide invaluable information about the influence of Alex® upon late-time chemical reactions in Tritonal. If the higher combustion rate of Alex® significantly affects bubble formation (or 'blast', were the detonation to occur in air), the result will be immediately apparent in the photographs. DSTO has also recently developed a novel application for aquarium tests of aluminised explosives by adjusting the high-speed camera to record light emitted from the burning aluminium [13], thereby allowing measurement of the rate of aluminium combustion within a detonating solid explosive. The DSTO experiments on Tritonal variants are the *first time* aquarium tests have been used expressly for this purpose, and are one of only a few methods capable of measuring any type of chemical reaction rate in a *solid* explosive *during detonation* and immediately thereafter.

3.1 Experimental setup

Aquarium tests were performed on 200mm long charges of TNT (2" dia) and Tritonal variants (1" and 2" dia). Charges were boostered with right cylinders of Pentolite of matching diameter, and initiated with RISI 501 EBW detonators.

Figure 3. Aquarium test setup in the 5kg high-explosives firing chamber. The charge (effigy shown) is suspended in the centre of a glass aquarium (on white stand). The image is diverted to a high-speed camera outside the chamber on the LHS by a mirror (centre right). The lights (yellow stand) and expensive video equipment (behind the mirror) are removed before firing.

Charges were immersed horizontally in a 400mm × 400mm × 600mm water-filled glass aquarium. The aquarium was marked with a 50mm × 50mm reference grid, and fitted with two PF-300 flash bulbs and a light diffuser to illuminate the water shock wave. High-speed frame photographs and streak images of the underwater detonations were taken with a Hadland Imacon 468 CCD camera. Camera exposures were generally timed to take four images of the detonation front travelling through the charge, and three images of the expanding bubble. Streak records were taken with a 100μm slit aperture oriented along the charge axis. The experimental setup is shown in Fig. 3.

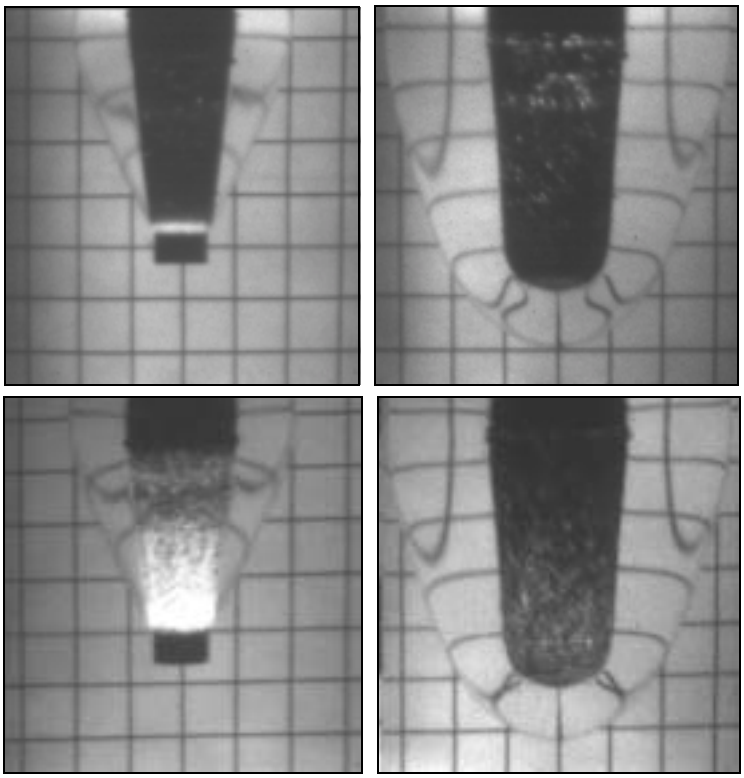

Figure 4. Aquarium test photographs of Tritonal charges made with Cap45a (top) and Alex® (bottom). Images were taken approximately 37μs (left) and 66μs (right) after initiation.

3.2 Results and analysis

3.2.1 Initial observations

For detonations in air, photography is generally only useful for recording the progress of the front of the detonation wave and the front of the 'fireball' that follows. It is difficult to record details of the reactions that occur within the fireball, since the detonation products tend to burn brightly. In aquarium tests, however, the water tends to cool and contain most of the detonation products, so that for aluminised explosives, only the illumination from the burning metal remains bright.

Frame images of aquarium tests of 2" diameter Tritonal variants (Fig. 4) show marked differences between the detonation reactions of the TNT/Cap45a and the TNT/Alex® formulations. For conventional Tritonal, burning of the Cap45a particles is evident as small points of light that become visible within the expanding detonation products long after the detonation front has passed.[1] In stark contrast, light emission for the Alex®-based Tritonal occurs immediately after the detonation front and quickly diminishes.

3.2.2 Analysis of streak images

Streak analysis of these aquarium tests provides quantitative estimates of Tritonal detonation velocities and pressures, and rates of aluminium combustion.

3.2.2.1 Detonation velocities and combustion rates

Streak images of aquarium tests of aluminised explosives can also capture the light from the burning aluminium, and it is from this that an estimate of the rates of aluminium combustion can be obtained. Streak analysis of TNT/Cap45a detonation shows that strong luminosity from Cap45a combustion occurs approximately 25μs after the detonation front, and persists beyond the maximum duration of imaging (100μs). Similar time patterns for light emission have been observed in aquarium tests of other explosives containing Cap45a [13]. During detonation of TNT/Alex®, however, the light from the burning Alex® appears *immediately* after the detonation front, and persists for only about 17μs, peaking at around 8 μs. If the light intensity is proportional to the amount of aluminium reacting, then these results indicate that for Tritonal detonation, most of the Alex® is consumed long before significant combustion of Cap45a occurs.

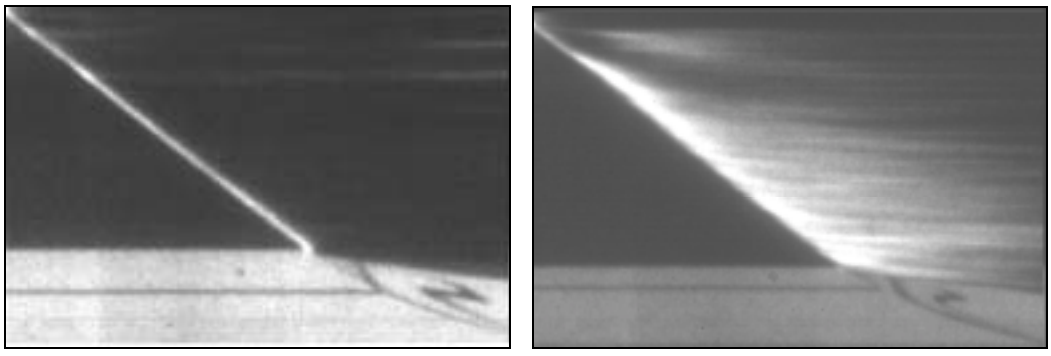

Figure 5. Streak images of the aquarium tests of Tritonal formulations containing Cap45a (left) and Alex® (right). In the left photograph, light from the burning Cap45a appears as horizontal traces in the top right corner.

[1] Light appearing after the detonation front is attributed to burning aluminium since no late-time illumination was observed in identical aquarium tests of neat TNT charges.

Detonation velocities of the Tritonal variants obtained from the aquarium tests are listed in Table 1. For the 2" (50.8mm) diameter charges, similar VoDs are obtained for TNT/Cap45a and TNT/Alex® formulations, while for the 1" (25.4mm) diameter charges, slightly higher detonation velocities are observed for the Alex®-based formulation. VoDs obtained from the aquarium tests are slightly higher than previous measurements of Tritonal detonations in air; it is likely these differences are due to the effects of water confinement.

Table 1. Streak analysis of the aquarium tests

Explosive[a]	**Event No.**[b]	**charge density (g/cm^3)**	**VoD (mm/μs)**	**Ave. VoD (mm/μs)**	**Shock**[c] **angle (deg.)**	**P_{CJ} (Gpa)**	**Ave. P_{CJ} (Gpa)**
1" (25.4mm)	**1**	1.75	6.530	6.585	39.5	17.9	16.6
TNT/Cap45a	**11**	1.75	6.652	± .062	36.3	16.8	±1.37
	12	1.75	6.573		55.6	15.2	
1" (25.4mm)	**2**	1.77	6.705	6.717	39.9	18.5	18.7
TNT/Alex®	**13**	1.77	6.698	±.028	41.8	19.4	±0.68
	14	1.77	6.749		57.6	18.1	
2" (50.8mm)	**3**	1.77	6.815	6.797	38.8	19.8	20.2
TNT/Cap45a	**7**	1.77	6.847	± .060	39.4	21.4	±1.04
	8	1.77	6.730		53.1	19.5	
2" (50.8mm)	**4**	1.77	6.897	6.800	41.0	23.4	23.4
TNT/Alex®	**5**	1.77	6.794	± .094	41.0	23.8	±0.35
	6	1.77	6.710		46.5	23.1	
2" (50.8mm)	**9**	1.56	6.752	6.650	37.6	17.8	17.5
'cast cloudy' TNT	**10**	1.56	6.549	± .143	37.0	17.0	±0.62

[a] All Tritonal variants are 80:20 TNT/aluminium.

[b] The event number serves as an index for the aquarium test images, representing the sequence in which the shots were fired.

[c] The angle of the exiting shock with respect to the bottom surface of the charge.

3.2.2.2 Detonation pressures

A rough estimate of the detonation or Chapman-Jouguet pressure[2] may be obtained from a measurement of the shock velocity as it enters the water at the end of the charge (lower half of streak photographs in Fig. 5). Assuming the pressure of the shock front is maintained across the interface between the explosive and the water, the shock pressure is then given by the relation:

$$P_{CJ} = P_S = U_S \rho_0 (U_S - C_0) / s \,, \qquad (1)$$

[2] The Chapman-Jouguet pressure is defined at a point following the detonation front where the detonation products are expanding at the speed of sound for the product material.

where P_S is the shock pressure, U_S is the shock velocity, and ρ_0, C_0 and s are empirical constants describing the shock properties of water (ρ_0=0.998 g/cm^3, C_0=1.647 mm/μs and s=1.921). A complete derivation of Equation 1 is given in Appendix B.

For this analysis, the water shock velocity U_S was derived from the initial slope of the curved shadow produced by the exiting water shock with respect to the bottom edge of the charge. These angles and estimates for detonation pressure are listed in Table 1. It is important to note that the primary aim of the aquarium tests - to image the light from aluminium combustion – required relatively large frame exposures and slit widths. This resulted in a subsequent loss of both spatial and temporal resolution for imaging the water shock, leading to large uncertainties in the measurement of the exiting angle of shock front, and hence to the associated estimates of detonation pressure. Therefore the P_{CJ} values listed in Table 1 should be used only as an indicator of general trends.

3.2.3 Analysis of frame photographs

The frame photographs of the aquarium tests are where properties of late-time reactions following the detonation front become apparent. It is primarily these reactions that affect formation of the bubble of detonation gases. Hence, any differences in the shape of the water shock or gas bubble produced by the different Tritonal variants signals a significant change to late-time detonation reactions caused by the replacement of Cap45a with Alex®.

Furthermore, the experimental shock and bubble profiles may be directly compared to the results of 2-dimensional hydrocode simulations of detonation. In this regard, aquarium tests are particularly useful for generating detailed information on the effects of non-ideal detonation, a phenomenon that is generally difficult to model.

3.2.3.1 Water shock and bubble profiles

Water shock and bubble profiles were measured directly from the frame photographs. The uncertainties in these measurements are due to image pixellation, and to relatively long exposure times, which lead to slight ‘smearing’ of the moving shock and bubble fronts. The limit of data resolution due to pixellation is 1mm; the uncertainty in position due to long exposures is between 1mm and 2mm, depending upon the speed of the wavefront.

A significantly larger experimental error exists due to an uncertainty of up to 2.5 μs in the timing of the initiation system. Hence, although the timing of the images can be specified to a precision of ±0.001 μs from initiation, the positions of detonation fronts of the same formulation taken ‘at the same time’ in successive experiments can differ by as much as 17mm. In order to compare profiles from different experiments measured at similar times, data sets were shifted to match the positions of detonation fronts. In some cases, variations in the initiation times led to large differences between profile shapes 100mm or more behind the shock front; these data were omitted from

subsequent curve fits of the profiles. Some data sets were also rotated (typically by a few tenths of a degree) to correct for slight tilt in charge positions.

A comparison of shock and bubble formation between conventional and Alex®-based Tritonal formulations can be made by directly overlaying profiles like those shown in Fig. 6. Since the profiles of two formulations are quite similar, curve-fitting of the data was generally required to discern any subtle differences within the experimental scatter; good fits of the data were obtained with fourth-order polynomial equations. The fitted profiles are plotted for comparison in Figures 7 and 8. The coefficients for the resulting polynomial fits are given in Table 2.

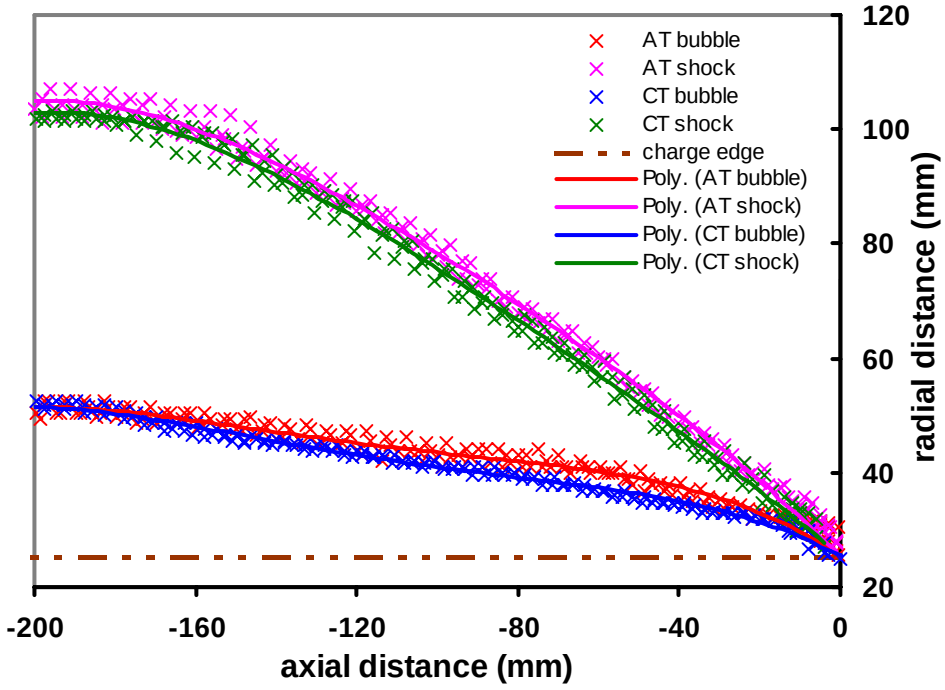

Figure 6. Shock and bubble profiles for detonation of Alex®-Tritonal (AT) andCap45a Tritonal (CT) approximately 37μs after initiation. Experimental data are shown as points, empirical polynomial (Poly.) curve fits as solid lines, and the original position of the charge edge as a dashed line. All profiles have been translated in the 'x' direction so that the shock front exits the charge at x = 0. Curve fits are fixed at the intercept (0mm, 25.4mm).

The fitted profiles are nearly identical, with the only differences suggesting a slightly greater rate of expansion in the shock and bubble profiles of Alex®-Tritonal detonations. All-in-all, the faster combustion rate of Alex® has little effect on bubble formation for Tritonal. This results complement recent blast tests of Tritonal variants which show that replacement of conventional aluminium with Alex® does not significantly affect blast performance [8, 14].

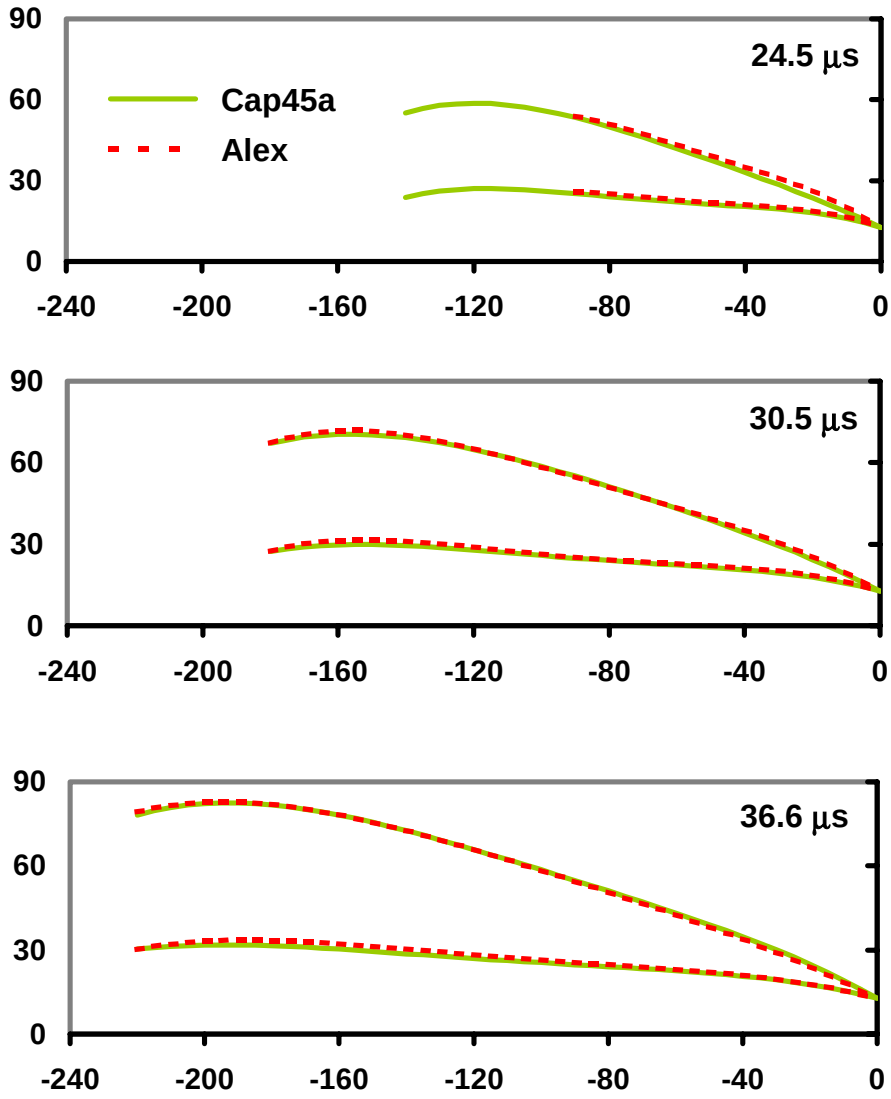

Figure 7. Comparison of fitted shock and bubble profiles for 1" Tritonal charges at various times after initiation. Axial and radial distances are shown in mm.

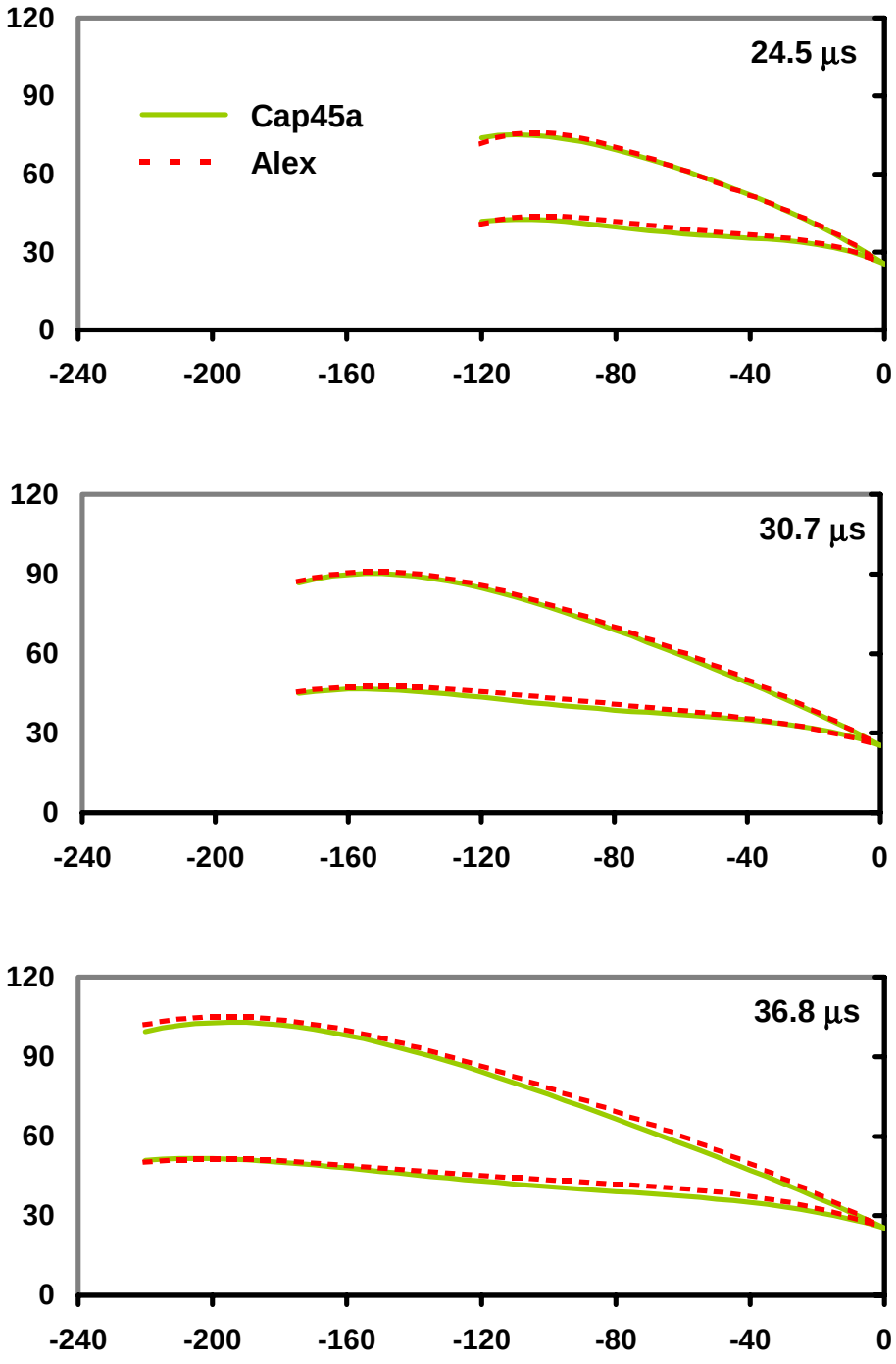

Figure 8. Comparison of fitted shock and bubble profiles for 2" Tritonal charges at various times after initiation. Axial and radial distances are shown in mm.

Table 2. Coefficients for curve fits of the shock and bubble profiles for the Tritonal variants. Curve fits are fourth-order polynomials of the form $y = ax^4 + bx^3 + cx^2 + dx + e$.

explosive	Δt (μs)	**profile**	a ($\times 10^{-7}$) (mm^{-3})	b ($\times 10^{-5}$) (mm^{-2})	c ($\times 10^{-3}$) (mm^{-1})	d	e (mm)
1" TNT / Cap45a	24.3	*shock*	-2.2184	-4.1352	-3.5569	-0.59824	12.7
		bubble	-3.1753	-8.4293	-7.7873	-0.38815	″
	30.5	*shock*	-0.98052	-2.6886	-3.5686	-0.64503	″
		bubble	-1.1950	-4.1593	-5.0520	0.33985	″
	36.6	*shock*	-0.80435	-2.9992	-4.4800	-0.68758	″
		bubble	-0.50112	-2.2388	-3.5343	-0.30743	″
1" TNT / Alex®	24.3	*shock*	-9.6461	-19.893	-15.141	-0.91236	″
		bubble	-6.3760	-14.548	-11.675	-0.48437	″
	30.5	*shock*	-1.8346	-5.7812	-7.0593	-0.76962	″
		bubble	-1.8555	-6.3859	-7.3607	-0.41967	″
	36.6	*shock*	-0.63150	-2.2241	-3.3346	-0.63246	″
		bubble	-0.62767	-2.6464	-3.9048	-0.32640	″
2" TNT / Cap45a	24.5	*shock*	-3.3377	-7.0031	-7.4669	-0.86937	25.4
		bubble	-6.3748	-16.2387	-14.1410	-0.59556	″
	30.7	*shock*	-0.94279	-2.1182	-2.6359	-0.66811	″
		bubble	-1.6082	-5.6872	-6.8674	-0.43368	″
	36.8	*shock*	-0.47288	-1.3168	-1.8012	-0.59890	″
		bubble	-0.61850	-2.8198	-4.3790	-0.37336	″
2" TNT / Alex®	24.5	*shock*	-8.0044	-16.6331	-13.4592	0.98668	″
		bubble	-7.7167	-18.4300	-15.3974	-0.65263	″
	30.7	*shock*	-1.0937	-2.7635	-3.6805	-0.73619	″
		bubble	-1.0941	-3.7230	-4.7527	-0.39256	″
	36.8	*shock*	-0.54873	-1.8816	-3.1258	-0.70961	″
		bubble	-0.69666	-3.3077	-5.5552	-0.47555	″

3.2.3.2 Radial pressures

The pressure of the shock front as it exits radially from the charge can be estimated from the angle θ_r between the shock front and cylinder axis [11,12]. In this case the relationship is given by

$$P_R = V_d \tan \theta_R \; \rho_0 (V_d \tan \theta_R - C_0) / s, \qquad (2)$$

where V_d is the detonation velocity.

In these tests, CCD bleaching from the light emission of the burning aluminium coupled with the lower spatial resolution of the imaging led to such a large uncertainty in θ_R that no consistent value for radial pressure could be obtained from direct measurements off the photographs. Therefore the angle was estimated by determining the slope of the curve fits for the shock front at the edge of the charge. The radial pressures determined by this method are listed below in Table 3. Even with this method, the estimates are inconsistent, but suggest that the radial pressures for the Alex®-based Tritonal are higher than those for the conventional formulation.

Table 3. Estimated radial pressures for Tritonal formulations

explosive	Δt (μs)	P_R (GPa)	explosive	Δt (μs)	P_R (GPa)
1” TNT / Cap45a	24.5	11.4	2” TNT / Cap45a	24.5	23.2
	30.5	13.0		30.7	14.6
	36.6	14.5		36.8	12.1
1” TNT / Alex®	24.5	24.8	2” TNT / Alex®	24.5	17.6
	30.5	18.3		30.7	17.3
	36.6	13.0		36.8	16.2

3.2.4 Patterns of light emission during aluminium combustion

A close inspection of the frame photographs reveals a detail of criss-cross patterns of light in or on the expanding bubble. Although these patterns can be discerned to some extent in the detonation of 2” diameter charges (Fig. 4), they are more readily apparent in the detonation of the smaller 1” diameter charges (Fig. 9).

The illumination pattern for the TNT / Alex® charge has a finer structure than that for TNT / Cap45a. It is possible these patterns are due to layering of aluminium particles within the TNT matrix; this type of layering was detected by scanning electron microscopy of Tritonal formulations containing Cap45a [6]. However, similar layering effects within Alex®-Tritonal formulations have not been reported.

Features of these illumination patterns are reminiscent of the soot traces on glass or the etching of metal surfaces produced by detonation instabilities in the form of transverse waves on the detonation front [15]. The patterns are also similar to transverse wave patterns in non-ideal detonation of TNT recorded by Howe *et al.* using optical techniques [16]. From their measurements, Howe *et al.* determined that the transverse wave patterns became coarser as the detonation became more unstable. If the patterns of light illumination in Tritonal are produced by transverse waves, then the following conclusions can be made by extrapolating from the results of Howe *et al.*:

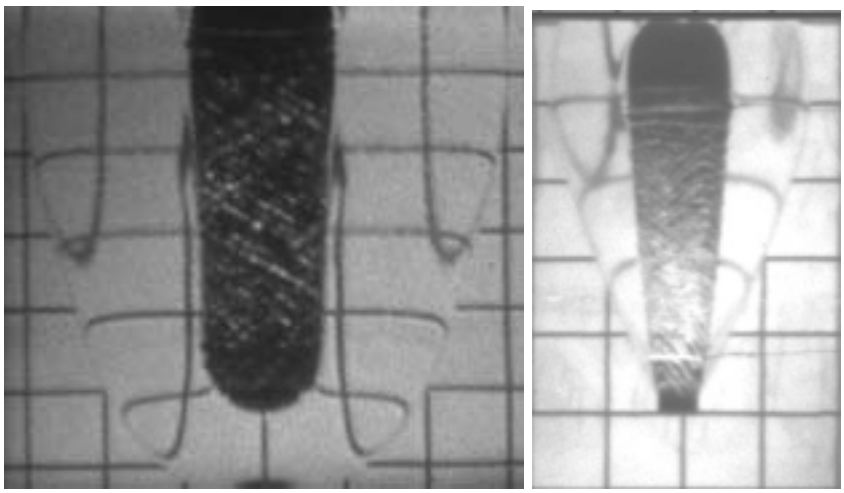

Figure 9. Illumination patterns in aluminium combustion observed for 1" (25.4mm) diameter charges of TNT/Cap45a (left) and TNT/Alex® (right).

- small-diameter Tritonal charges are prone to detonation instabilities;
- at any given charge diameter, detonation of Alex®-Tritonal is more stable than that of Tritonal made with Cap45a; and
- Alex®-Tritonal has a smaller failure diameter than conventional Tritonal.

The last point was predicted at a recent defence science symposium [9], and later tested and confirmed by other researchers [8b]. A comprehensive set of critical diameter tests on Tritonal are currently being conducted at DSTO, and the results will be reported in separate publication.

A more detailed discussion of how the higher rate of aluminium combustion may affect the detonation stability of Tritonal will be given in Section 5.

3.3 Further comments and recommendations

The aquarium tests provide an excellent visual comparison of the different combustion rates of aluminium powders in explosives, and vivid evidence that Alex® ignites almost immediately after the detonation front, thus supporting the hypothesis that it burns fast enough to influence properties of detonation. Given the success and the relatively simplicity of these experiments, aquarium tests will be used to investigate the combustion of other grades of aluminium powders in various solid explosives. These tests will provide a comprehensive data set that can be used to validate reaction rate models for aluminised explosives. There is every reason to expect that aquarium tests will also generate useful combustion data for other metal fuels that burn fast and bright in solid materials, and that these tests can be performed for propellant and pyrotechnic compositions as well as explosives.

One drawback of the aquarium tests in this configuration is the uncertainty associated with pressure estimates, due in part to the low resolution resulting from the longer exposure times forequired to image the light from the burning aluminium. If pressure measurements are the ultimate aim of the experiment, then the resolution of the images must be increased. This can be achieved by modifying the camera aperture, decreasing the slit widths, or reducing image exposure times. Better resolution may also be obtained using a film-based high-speed camera.

A drawback of using aquarium test to measure pressure is that no specific portion of the water shock profile has been identified as that best suited for deriving the pressure information. Therefore, a useful and informative exercise would be use a alternative method to measure pressure (*eg.*, manganin gauges) in an aquarium test to provide simultaneous and comparable data of the same phenomenon. From this, the proper pressure interpretation of aquarium test photographs can be ascertained. Failing that, pressure information can be derived indirectly from aquarium tests by comparison to hydrocode simulations.

4. Detonation Front Curvature Measurements

Alex®-induced performance enhancement of Tritonal is greatest under conditions of 'non-ideal' detonation. During non-ideal detonation, the detonation front is subject to energy losses that degrade performance and exaggerate the effects of charge size and shape. In small cylindrical sticks of explosives, an obvious manifestation of non-ideal detonation is the appearance of a curved detonation front. The curvature arises from energy losses at the edge of the cylinder that cause the sides of the detonation front to lag behind the center. As the diameter of the cylinder is reduced (or alternatively the detonation becomes more 'non-ideal'), energy losses increase and the detonation front curvature becomes more pronounced. It is reasonable to assume that faster combustion of Alex® may compensate for these energy losses, leading to a reduction in detonation front curvature with respect to conventional Tritonal.

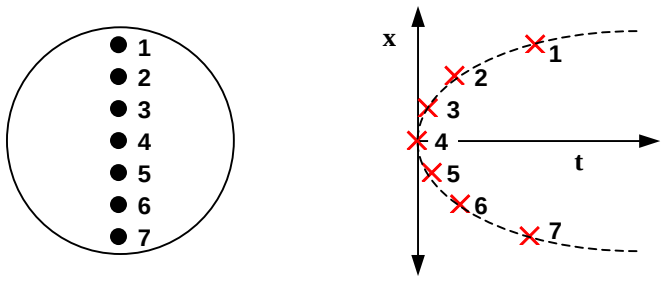

Figure 10. Detonation front curvature measurement using piezoelectric array. The array (left) records the times when the shock front hits each pin, resulting in a measurement of the time lag (right) between the centre (pin 4) and the edges (pins 1 and 7) of the shock front.

A good way to image the shape of detonation front within an explosive charge is with flash x-ray photography. However, an often cheaper or more convenient alternative is to measure the shock front as it exits the explosive. For a large charge, this can be achieved by using an array of piezoelectric pins fastened to the end of the explosive as in Fig. 10.

An alternative method of measuring breakout is to use 'flash gaps,' which take advantage of the fact that some gases emit light when subjected to shock waves. One such gas – argon - is present in the atmosphere (0.93% by volume), so that ordinary air will visibly luminesce under large shocks. Hence a 'flash gap' may be fabricated by simply trapping a small amount of air between the end of an explosive and a transparent plate. Aligning the slit of a streak camera across the plate will then produce a distance-time trace for the detonation front analogous to that of the piezopin array shown above in Fig. 10.

Like the piezopin array, a flash gap is a simple, inexpensive and non-intrusive technique for measuring detonation curvature, particularly in small charges where the effects of non-ideal detonation are enhanced. Further discussion of flash gap arrays and their application to detonation front curvature measurements of HMX and TATB formulations may be found in Chéret [17] and references therein.

4.1 Experimental setup

Detonation curvature measurements were performed on 250mm charges of TNT (1" diameter) and Tritonal variants (1" and 2" diameter). Charges were boostered with right cylinders of Pentolite of matching diameter, and initiated with RISI 501 EBW detonators.

Flash gaps were fabricated by machining a shallow cylindrical hollow into one face of a 1"or 2" diameter Perspex disk, leaving a 2-3mm lip to serve as an adhesive surface. Optimal thicknesses for the Perspex disks and the flash gaps will depend upon the performance of the explosive.[3] For explosive formulations that generate relatively low shock pressures, it is recommended that the air in the flash gas be enriched with argon. For this experiment, disks 5mm thick were fabricated with gaps of 0.1mm, 0.2mm and 0.5mm. Initial shots were fired with the 0.5mm flash gaps (those containing the most gas), but it was found that the 0.1mm and 0.2mm flash gaps emitted sufficient light and yielded 'cleaner' streak records. Argon enrichment of the flash gaps was attempted, but no significant improvements in the resulting streak images were observed.

In these measurements, two flash gaps were attached to the end of the charge using Araldite® epoxy. To derive the spatial curvature of the wavefront from the recorded time lag, an accurate value for detonation velocity is required. Since our only streak camera was already employed to monitor the flash gaps, the detonation velocity was

[3] The intensity of the flash depends upon the detonation pressure of the explosive, and the thickness of the disk will determine the time separation between successive flashes in an array of two or more flash gaps. Thus smaller flash gaps in thicker disks should be used for high-performance explosives with relatively high detonation velocities.

measured using a standard piezoelectric pin array, consisting of 8 to 10 pins spaced 20 or 25mm apart. The array was epoxied to the charge so that the pin furthest from the booster was 5mm from the end face. A schematic of the experimental setup is shown in Fig. 11.

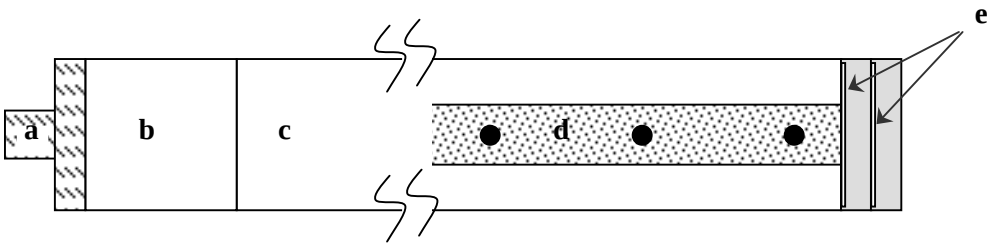

Figure 11. Schematic of 1" diameter charge and flash gap array for detonation curvature measurements: (a) holder for EBW detonator, (b) pentolite booster (c) main charge (d) piezoelectric pin array, and (e) Perspex flash gaps.

4.2 Results and analysis

4.2.1 Initial observations

Streak records generated by the Perspex flash gap arrays are shown in Figures 12 and 13. The greyscale has been inverted in both images to enhance detail. The pattern shown in Fig. 12 is similar to those generated by other flash gap arrays [17], and is the shape expected for a detonation front that leads at the centre of the charge, and lags at the edges[4]. In this image, the light produced by the first flash gap (far left curve) was bright enough to saturate the CCD elements[5], causing a slight vertical smearing of the front pattern. The detonation curvature is enhanced in the following signal from the second flash gap. This is because the lower-pressure edges of the detonation front travel more slowly through the first Perspex disk, and therefore lag farther behind the centre in the second flash gap[6]. A short time after the detonation front travels across the flash gaps, the detonation products burn through the Perspex disks, causing the 'smudge' of light from the centre of the image to the right hand side. Light from the expanding gases is also evident as diagonal streaks emanating from the signal of the second flash gap towards the right-hand corners.

[4] The reader is referred to Appendix A for a detailed explanation of the interpretation of streak records for flash gap detonation front curvature measurements.

[5] A CCD camera transforms a light pattern into an electric image via a two-dimensional array of light-collecting elements. Intense light will saturate these elements, causing the signal to overflow into adjacent sensors, which results in 'smearing' of the detected light pattern.

[6] There is no direct way to estimate detonation front pressure from these measurements, however, these results could be simulated in hydrocodes.

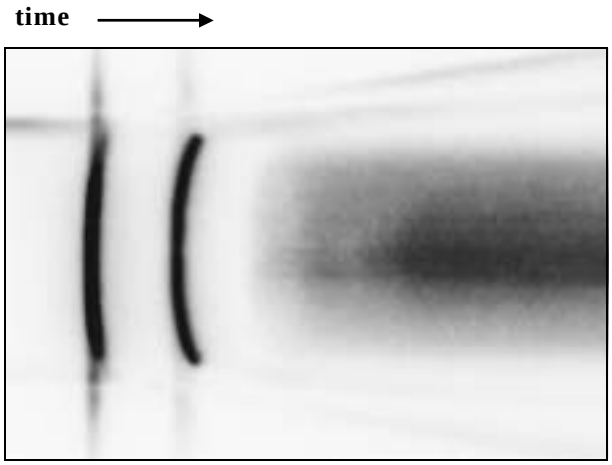

Figure 12. Streak record of a 'typical' detonation front exiting a 1" diameter charge of TNT/Cap45a. The curvature of the detonation front was captured using two 0.2mm Perspex flash gaps attached to the end of the charge.

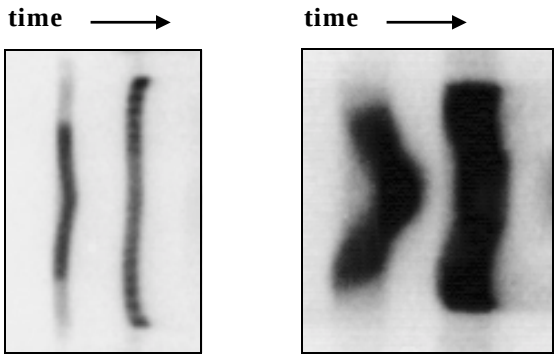

Figure 13. 'Unusual' detonation curvature measurements recorded for TNT/Alex® charges. Shown are detonation fronts recorded for (left) a 2" diameter charge using 0.2mm flash gaps, and (right) a 1" diameter charge using 0.5mm flash gaps.

The shape of the detonation fronts shown in Fig. 13 are unexpected in that the centre of the front lags behind the edges, particularly in the first flash gap. However, this initial lag does not correspond necessarily to a lower front pressure, since the centre curvature decreases by the time the front reaches the second flash gap. This streak pattern was produced consistently by both the 1" and 2" diameter charges of Alex®-based Tritonal, but not by the conventional Tritonal. Similar unconventional shapes have been observed in detonation fronts measured for other explosives [18] and are attributed to the presence of cavities or defects within the charges. It is likely that the 'dimple' in the Alex®-Tritonal detonation fronts is produced by a central cavity or 'coring' within the charges. Alex®-Tritonal formulations are prone to coring, and an extreme example of this is shown in a previous technical report [6].

4.2.2 Detonation velocities from piezoelectric pin arrays

Detonation velocities measured for the Tritonal and TNT charges using piezoelectric pin arrays are listed in Table 4 below. VoDs obtained for the Tritonal formulations generally agree with previous results, except for those of the 1" diameter charges of 'conventional' Tritonal, which are significantly higher. Given that the measurement was reasonably consistent over the three shots, and no defects were detected either on the arrays or in the output signals, there is as yet no obvious reason for this discrepancy. A failing detonation was observed in all three 1" charges of 'cast-cloudy' TNT. Therefore the values for detonation velocities listed in Table 4 serve only to represent the average detonation velocity measured across the piezopin array. A plot of the signals from the piezoelectric array detailing the behaviour of the failing detonation in the 1" TNT charges is given in Fig. 14. One of the Perspex flash gaps was recovered undamaged for Event 30.

Table 4. Measured detonation velocities of Tritonal variants and 'cast cloudy' TNT.

Explosive	**Event**	**density (g/cm^3)**	**VoD (mm/μs)**	**Ave. VoD (mm/μs)**
1" (25.4mm) TNT/Cap45a	**18**	1.78	6.771	6.752 ± .033
	26	1.78	6.714	
	27	1.77	6.772	
1" (25.4mm) TNT/Alex®	**19**	1.77	6.762	6.776 ± .034
	25	1.77	6.752	
	28	1.77	6.814	
2" (50.8mm) TNT/Cap45a	**16**	1.77	6.859	6.848 ± .126
	17	1.76	6.717	
	22	1.77	6.968	
2" (50.8mm) TNT/Alex®	**21**	1.77	6.811	6.818 ± .015
	23	1.77	6.807	
	24	1.77	6.834	
1" (24.5mm) TNT	**20**	1.56	4.894	*failing detonation*
	29	1.56	4.762	
	30	1.56	-	

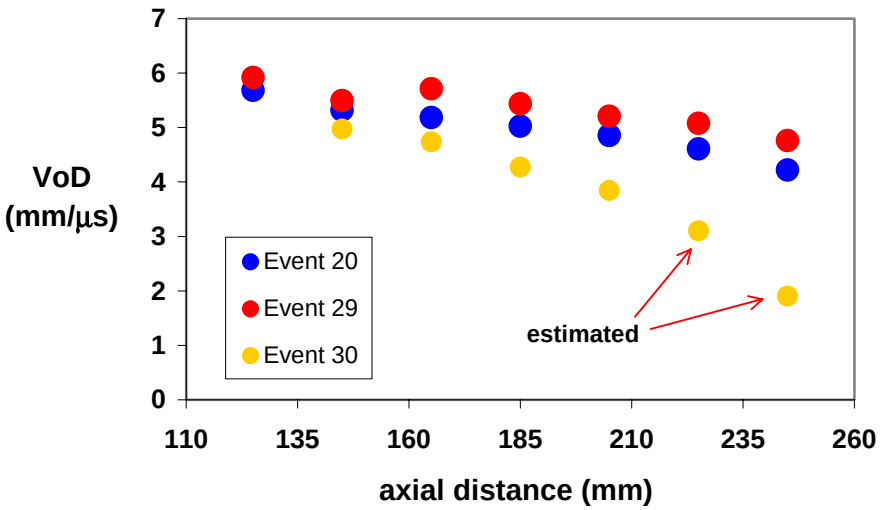

Figure 14. Plot of measured VoDs showing detonation failure in 1" (25.4mm) diameter charges of 'cast-cloudy' TNT.

4.2.3 Detonation curvature measurements from the streak records

The shape of the detonation front as recorded by the first flash gap (nearest the charge) was measured directly from the streak photograph, and converted from time lag *dt* to spatial lag *dy* using the relation

$$dy = V_d\, dt \qquad (3)$$

where V_d are the detonation velocities listed in Table 4. Measurements from 'good' streak records (like that of Fig. 12) for TNT and Tritonal are plotted in Fig. 15. For this exercise, the data have translated to shift the centre of the detonation front to $x, y = 0$. A rudimentary assessment[7] of the detonation front curvature takes the form of the radius of curvature, R_d [8], obtained by fitting the graph to the curve

$$y = R_d - \sqrt{R_d^{\,2} - x^2}\ . \qquad (4)$$

The observed trends of detonation front curvature in conventional Tritonal are as expected: the smaller the charge, the more non-ideal the detonation and the greater the detonation front curvature. Indeed, the measured curvature in the 1" Tritonal charges is nearly equal to that of the failing detonation front in 1" TNT.

[7] Several techniques have been developed to analyse detonation front curvature, and often the analysis is divided into two parts to assess (1) the curvature at the centre of the front, which gives information about the detonation reaction zone, and (2) the shape of the trailing edges, which gives information about side losses. In these cases, the data may be translated and rotated in space to obtain a reasonable fit. See Cooper [10], Chéret [17], or Souers and Garza [18] for further discussion.

[8] Note that R_d is *inversely* proportional to curvature, *i.e.*, a low R_d corresponds to high curvature.

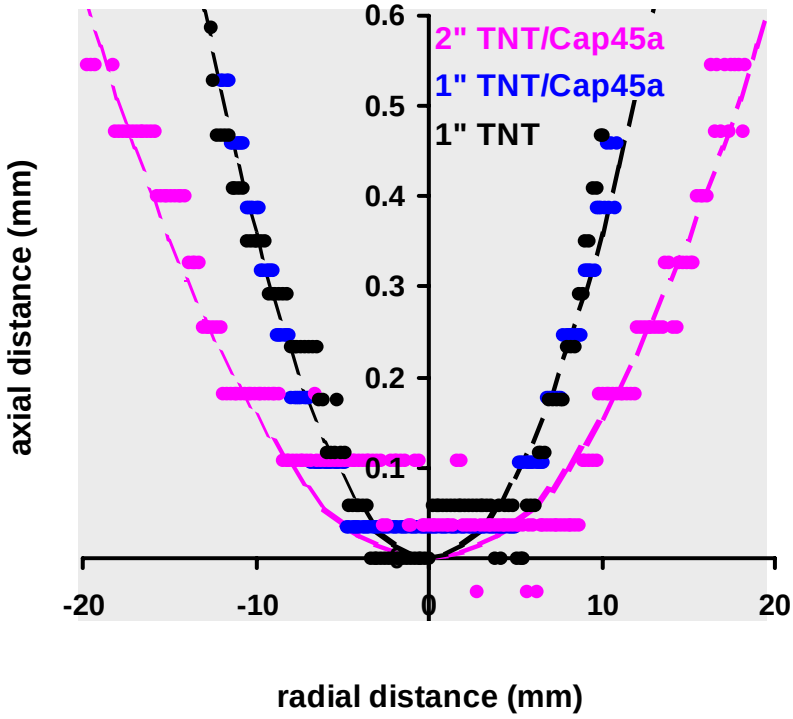

Figure 15. Detonation front curvature profiles of TNT and Tritonal (80:20 TNT/Cap45a) measured from streak images of flash gap signals. Data are shown as filled circles, and curve fits as dashed lines.

Unfortunately, the results of these tests were not consistent enough to provide firm quantitative measurements from the streak images. All of the detonation fronts of the Alex®-based Tritonal charges were similar to that in Fig. 13, and could therefore not be fitted to a single-valued radius of curvature, R_d. For the 'conventional' Tritonal formulations containing Cap45a, only two of the three shots gave similar results for each of the two diameters, and for TNT, only one streak image captured the front of the failing detonation. Given the scatter of the available data, the estimated uncertainty in R_d is around 10%. The results are summarised below in Table 5.

Table 5. Measured and reported values for detonation curvature in Tritonal containing Cap45a and TNT. The estimated uncertainty in R_d is approximately ±10%.

Explosive	**Charge dia**	***R_d* (mm)**	
		this experiment	*reported*
TNT	1"	140 [a]	--
	2"	*(expect R_d > 140)*	140 [c], 102 [d]
Tritonal	1"	140 [b]	--
	2"	320 [b]	125 [c], 144 [d]

[a] measured from one event
[b] measured from two events
[c] from Ref. 41
[d] from Ref. 27

The magnitudes of the detonation curvatures obtained in these experiments do not agree with previously reported values. For instance, the curvature measured for the 2" charges of 80:20 TNT/Cap45a (R_d ~ 320mm), is much lower than that reported for conventional Tritonal (R_d ~ 140mm). Similarly, the curvature measured for failing (*i.e.*, 'highly non-ideal') detonation in 1" TNT is identical to that reported for steady detonation in 2" TNT, whereas one would expect a lower curvature in the larger charge, which supports a more 'ideal' detonation.

Although these experiments produced several apparently anomalous results, there is, however, no reason to assume that all the curvature measurements obtained by the flash gaps are less valid than the literature values, many of which were obtained over 40 years ago. As mentioned previously, the 'non-ideal' properties of a detonation can depend quite sensitively upon the nature of the explosive ingredients and the method of charge fabrication. For instance, the Cap45a used in these experiments is likely to have a smaller average particle size than aluminium powders used in older formulations, which may lead to improved casting properties or better burn, which in turn stabilises the detonation.[9] Furhtermore, detonation front curvatures previously reported for TNT were obtained by extrapolation of data from pressed charges rather than from a direct measurement on cast charges, and may therefore not be comparable to these results.

4.3 Further comments and recommendations

Like the aquarium tests, the detonation front curvature tests suffer from low image resolution. The resolution is constrained by the uncertainty associated with the timing of the initiation system on the explosive train. That is, since the uncertainty associated with the initiator is on the order of 2.5 μs, the duration of the streak image was set greater than 5 μs to ensure capture of the flash gap signals. Hence, the curvature of the wavefront was typically described by less than 20 pixels along the time (or '*y*') axis. Despite this limitation, flash gaps provide more data than a piezoelectric pin array like that of Fig. 10, particularly for small charges.

Given the low resolution and the likelihood of rejecting measurements due to anomalies in the shape of the detonation front (*e.g.*, Fig. 13), five or more firings are recommended to obtain a good quantitative estimate of detonation front curvature in one charge configuration. It is also recommended that static X-ray images of the charges be taken to identify any internal flaws that may affect the shape of the detonation front.

Another limitation of the flash gaps is a loss of data at the edges of the detonation front because of the need for an adhesive surface to attach the disks to the end of the charge. Hence flash gaps may not be a good method to use if measurement of "side losses" at the edge of the charge is important.

[9] Indeed, Sandstrom *et al.* [41] note that observed detonation curvature and diameter effects for Tritonal were quite similar to TNT, and from this concluded that the aluminium component in the Tritonal "did not contribute significantly to the chemical reactions that sustain the detonation front."

Finally, although better images may obtained with optically transparent disks, this is not a requirement. Indeed, good streak records have been obtained with cloudy, unpolished disks or even disks that have been meticulously inked in with a black permanent marker (although this type of alteration is *not* recommended). Such an example serves to show that, besides being simple, inexpensive, and non-intrusive, the flash gap experiment is also quite robust.

5. A model for the influence of Alex® upon Tritonal

The physical and chemical behaviour of ultrafine aluminium powders and their effects upon explosive performance has been the topic of several studies since the advent of Alex® in the early 1990s. Despite early claims of its ability to significantly enhance the performance of energetic materials, it has generally been found that substitution of Alex® into aluminised high-explosive formulations results in relatively subtle changes in performance, be they beneficial or detrimental. These changes could arise from a variety of factors, including:

- the amount of active aluminium in the powders;
- the physical properties of the charge, such as charge density, mix homogeneity, and the presence of casting flaws;
- variations in detonation thermochemistry; and
- anomalies in the shock properties of the unreacted material.

However, there is a significant amount of evidence to suggest that most of the Alex®-induced changes in explosives performance can be explained by a simple general model of particle ignition and combustion with relatively coarse physico-chemical parameters such as detonation temperature and pressure. In the interest of clarity, only this model will be presented below.

5.1 General comments on particle size effects

For any chemical reaction, a primary factor controlling the rate at which the reaction proceeds is the amount of reactive material available. In solids, the reaction rate is strongly influenced by the amount of active surface material. Hence, the most effective way to increase the rate of combustion (*i.e.*, oxidation) of aluminium powders is to decrease the size of the aluminium particles, resulting in a greater amount of surface aluminium in contact with surrounding oxidisers (*eg.*, oxygen gas, ammonium perchlorate, or high explosives). Hence, an ultrafine aluminium powder such as Alex®, with an average particle size at least 100 times smaller than its conventional counterpart Cap54a, will burn much faster, a fact which is vividly demonstrated in the aquarium tests presented above.

The velocity of detonation in energetic materials is essentially a measure of the rate of fastest reaction in the detonation process. It is therefore tempting to attribute any relative increase in the detonation velocity of aluminised explosives containing Alex® simply to the higher rate of Alex® combustion. If this were the case, then substitution

of conventional aluminium by Alex® in any aluminised explosive should always result in an increase in detonation velocity. However, the detonation velocity of Alex®-based formulations can be higher, lower the same as their "conventional" counterparts, as shown in Table 6. Clearly, the effect of the higher Alex® reaction rate upon performance also depends upon the nature of the explosive.

Table 6. Reported change in the detonation velocities of aluminised explosives upon substitution of conventional (micrometric) Al by ultrafine (nanometric) Al.

Ref.	**formulation**	**change in VoD**
19, 20	HMX / binder	decrease
21	NM / PMMA / Al	decrease
7,22, 6	RDX / AP / Al / binder	same or slightly lower
	CL-20 / Al	same
19	BTNNA / Al	same
21, 6	TNT / Al	decrease[a] (from 1" cylinder tests); increase (from unconfined firings)
5	ADN / Al / binder	increase (from 4.086 to 6.160 mm / μs)
23	lactose / Al / AP	increase

[a] The density of the charges containing ultrafine Al (ρ =1.59 g / cc) was lower than that of the charges containing 5 μm Al (ρ =1.635 g / cc).

One trend apparent from Table 6 is that Alex® substitution tends to decrease or leave unaffected the detonation velocities of aluminised formulations containing a high percentage of high explosive ingredients (*eg.*, HMX and RDX), and increase the detonation velocity of formulations containing less powerful explosives such as ammonium dinitramide (ADN) or ammonium perchlorate (AP). These types of explosives generally have lower detonation velocities (and therefore lower reaction rates) and exhibit non-ideal detonation behaviour in the range of charge sizes generally used for laboratory testing. Also, whereas aluminium tends to behave as a diluent and reduce detonation performance of high-explosive formulations, in formulations such as ANFO, addition of aluminium - even as a coarse powder - *enhances* performance. This indicates that the rate of aluminium reaction is fast enough to contribute energy to the detonation front of AN or AP-based explosives (VoD ~ 1-2.5 mm / μs), but too slow to contribute energy to the detonation of high explosives (VoD ~ 7-8 mm / μs).

Indeed, particle size effects on the detonation performance of AN formulations are well documented for various grades of micrometric aluminium powders. An example of this was reported by Maranda *et. al.* [24] for 80:10:10 AN / TNT / Al mixtures containing either 300 μm powder or 160 μm flaked aluminium. Their results, represented below in Fig. 16, show that the formulation containing the finer aluminium powder yields higher detonation velocities for small diameter charges. Similar trends have been observed for the Tritonal variants [25], suggesting that reaction of the nanometric aluminium is fast enough to influence the detonation reaction of a high explosive (VoD ~ 6-7 mm / μs), albeit under non-ideal detonation conditions.

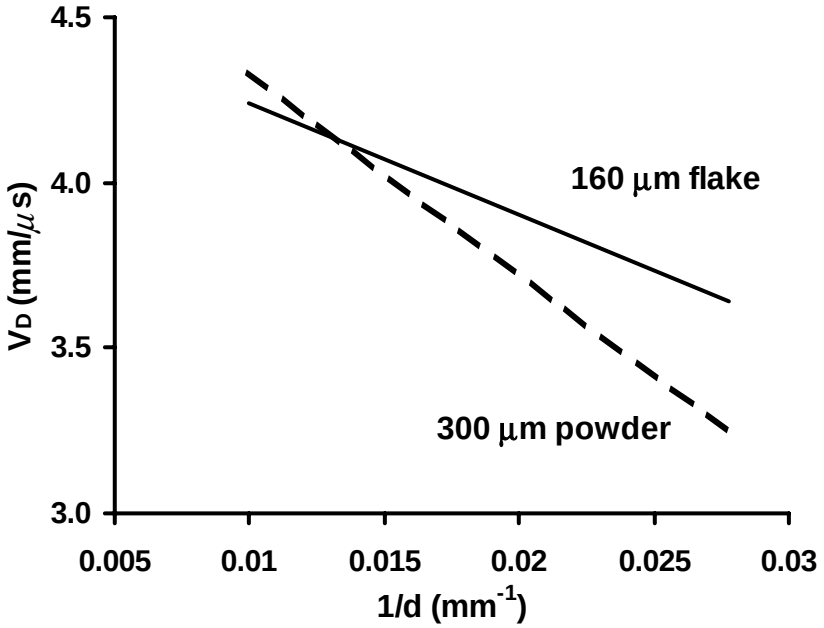

Figure 16. A representation of the results of Maranda et al. [24] showing the effect of particle size upon the detonation performance of 80:10:10 AN/TNT/Al formulations containing micrometric aluminium powder.

An intriguing result of Maranda *et. al.* is an apparent crossover of the detonation velocities that occurs near a charge diameter of 80mm: the formulation containing the coarser aluminium powder has a greater VoD at larger charge diameters (VoD > 4.1 mm/μs), where the explosive is expected to behave more "ideally." This result matches the trend in Table 6, and suggests that some general aspect of the aluminium reaction has a detrimental effect upon detonation velocity of this formulation - an effect that is enhanced by smaller particle sizes.

Often, detrimental effects resulting from the addition of aluminium to high-explosive formulations are attributed to Al acting as an inert ingredient, that is, the lower detonation performance is due to the reduction of "reactive" high explosive ingredients. However, careful studies by Cook and coworkers on TNT and TNT/RDX formulations [26] show that aluminium lowers detonation pressures and velocities even more than an ideal diluent; a representative set of results is listed in Table 7 below. This initial effective heat-absorbing reaction of Al during detonation has been observed several times for TNT-based [27,28] formulations, and at least once [22] for PBX formulations. Like the AN/TNT/Al formulations, the decrease in detonation velocities and pressures for large-diameter Tritonal charges is greater in formulations containing finer aluminium powders (see Table 8).

Table 7. The results of Cook et al. [26] showing the effect of adding Al or an "ideal" inert ingredient (NaCl) upon the detonation velocities of TNT-based formulations.

Explosive	Density (g/cc)	VoD (mm/us)
TNT	1.59	6.91
80:20 TNT/NaCl	1.75	6.90
80:20 TNT/Al	1.75	6.80
60:40 RDX/TNT	1.70	7.80
45:30:25 RDX/TNT/NaCl	1.77	7.43
45:30:25 RDX/TNT/Al	1.77	7.20

Table 8. The effects of the particle size of Al and SiO_2 powders upon TNT performance (from Dremin [28]).

Explosive	ρ_{exp} (g/cc)	ρ_{TNT} (g/cc)	dia (μm)	VoD (mm/μs)	U_S (mm/μs)	P_{CJ} (GPa)
85:15 TNT/Al	1.49	1.38	0.2	5.75	1.27	10.0
			80	6.20	1.45	13.4
			> 270	6.27	1.47	13.7
85:15 TNT/SiO_2	1.49	1.38	<0.2	5.98	1.51	13.5
			270	6.27	1.53	14.3
TNT		1.36	--	6.20	1.45	12.2
		1.59	--	6.91		15

The simplest explanation proposed for the initial endothermic effect of aluminium on detonation is that the reaction of Al particles takes place in two steps: ignition and combustion. Although aluminium is a highly energetic fuel, and its combustion a strongly exothermic reaction, the particles must first absorb enough energy to vaporise the metal and breach the non-reactive oxide coating (thus allowing contact between the active aluminium and the oxidant). Both the ignition energy and the time-to-ignition increases with the size of the particle and the thickness of the oxide coating, as demonstrated in extensive studies of particle ignition in fuel-air explosives [29] and, more recently, solid explosives [30]. This simple model suggests that it is possible for aluminium powders with small enough particle sizes to ignite and begin to burn within the reaction zones of high explosives, thereby contributing energy to the detonation front and enhancing detonation performance.[10]

[10] This is assuming that a high active metal content can be maintained in the nanometric powders. An alternative explanation for the observed relative decrease in the detonation performance of Alex-based HMX or RDX formulations is the lower percentage of active aluminium in the ultrafine powder (88-90% as opposed to 99% in conventional micron-sized powders.)

5.2 Alex® ignition and combustion in Tritonal

In the model discussed above, the reaction of aluminium during gaseous or condensed-phase detonation proceeds in the following steps:

1. The aluminium particles absorb shock and thermal energy from the detonation front.
2. The absorbed energy melts, vaporizes, cracks [31] or "blows away" [32] the oxide shell, and proceeds to melt and vaporize the active aluminium.
3. Upon reaching a certain temperature, the Al particles ignite and react with detonation products either within or following the detonation front.
4. Energy released by aluminium combustion increases the temperature and pressure of the detonation products.

The light from the burning aluminum imaged in the aquarium tests is clear evidence that the detonation conditions of Tritonal meet or exceed the ignition criteria of both Alex® and Cap45a. The detonation pressure of Tritonal is at least a thousand times greater than the pressures observed to breach oxide coatings on metal particles dispersed in oxygen gas flows [32b]. Likewise, the detonation temperature of TNT (between 2450 and 3200°C) is greater than the melting point of aluminium oxide (~2070°C), and high enough to vaporise the active aluminium within the particle (b.p. 2480°C).[11]

For the aluminium to enhance explosive performance, combustion of the particles (step 4) must begin within the detonation reaction zone. Assuming the detonation reaction zone of Tritonal is similar to that of TNT, the Al particles must ignite within 280 [34] to 330ns [35]. Studies, including this one, of alumininised explosives indicate that ignition of micrometric aluminium powders takes much longer than that. From high-speed photographs of the detonation of NM-PMMA/Al mixtures, Kato and Brochet [36] conclude that combustion of 8-15 μm aluminium particles occur after a delay of at least "several hundred nanoseconds"[12]. First-principles calculations of aluminium suspended in a hot gas (T=2700°C) estimate an ignition time of 12 μs for 5 μm particles [29b] and pressure measurements of ammonium nitrate formulations containing "fine" aluminium indicate particle ignition occurs approximately 4 μs after the detonation front [38]. Through careful measurements of particle size effects in aluminised ammonium nitrate formulations [39], Leiper and Cooper found that the dependence of aluminium time-to-ignition τ (in μs) upon particle diameter ϕ (in μm) was well described by the relation:

$$\tau \sim 0.5\, \phi^{0.5}. \qquad (5)$$

[11] Indeed, differential thermal analysis indicate that the onset of oxidation of aluminium powders occurs at much lower temperatures: approximately 980C for 9 um particles and 550-600C for 130nm aluminium powders. Approximately 50% of the ultrafine aluminium powder was oxidised before the sample reached the melting point of aluminium (660C) [33].

[12] Nevertheless, they also mention an earlier publication reporting an increase in brightness temperature over similar mixtures containing inert particles, which could be attributed to "combustion of [a] small part of Al at [the] C-J plane" [37].

From this, they calculated an ignition delay for paint-grade aluminium flake (100nm particle size) of 160-220 ns, in good agreement with their experimental value of 200ns ± 20ns, measured by optical and electromagnetic particle velocity gauge techniques. From this relationship, the estimated time-to-ignition for Alex® will be approximately 220ns - a delay short enough to allow some aluminium combustion within the reaction zone of TNT, and probably Tritonal as well.

After ignition, the combustion rate of ultrafine aluminium is greater than conventional aluminium. The higher rate of energy release generates higher temperatures and pressures within the detonation products. Pyrometric measurements of aluminised solid explosives indicate an increase of 100-1000°C in detonation temperatures for Alex®-based formulations, depending upon the aluminium content [22, 40]. Similarly, detonation pressures have been observed to increase by as much as 20-25% for both TNT [6] and AN-based formulations [38].

The higher rate of energy release with Alex® combustion can also serve to stabilise marginal detonations. For small charges near the failure diameter, energy losses due to gas expansion and shock rarefactions can undermine the detonation reaction, causing it to oscillate. Oscillations in the detonation front appear as transverse waves that produce criss-cross patterns in images of the detonation, similar to the patterns observed in 1” Tritonal charges (Fig. 9 on p. 14 above). The more unsteady the detonation, the larger the amplitude of the oscillations, and the coarser the transverse wave pattern. According to calculations of Howe *et al.* [16], higher rates of energy release serve to counteract these energy losses, and stabilise the detonation. Hence, a higher rate of energy release during a detonation reaction will result in a finer transverse wave pattern for a particular charge diameter, and a reduction in overall critical charge diameter.

Overall, substitution of conventional aluminum with Alex® Tritonal formulations leads to a 5-25% increase in the detonation performance of small charges (25 - 30mm dia), and a significant decrease in critical diameter. This suggests that Alex® could be used for stabilising detonation under extremely non-ideal conditions, and may therefore prove an invaluable ingredient for tailoring explosives to specific applications.

6. References

1. Katz J., Tepper F., Ivanov G.V., Lerner M.I., and Davidovich I. (1998) "Metastable Nanosize Aluminium Powder as a Reactant in Energetic Formulations," *Proc. of the JANNAF Propulsion Meeting* 15-17 July, Cleveland OH (USA), CPIA Publication 675, v3, 343-9.
2. Bashung B., Grune D., Licht H.H. and Samirant M. (2000) "Combustion Phenomena of a Solid Propellant Based on Aluminium Powder," *5th Int. Symp. on Special Topics in Chemical Propulsion*, 19-22 June, Stresa (Italy).
3. (a) Mench M.M., Kuo K.K., Yeh C.L. and Lu Y.C. (1998) "Comparison of Thermal Behaviour of Regular and Ultra-fine Aluminium Powders (Alex) Made from Plasma Explosion Process," *Comb. Sci. and Tech.* **135**, pp 269-92; (b) Mench M.M., Yeh C.L. and Kuo K.K. (1998) "Propellant Burning Rate Enhancement and Thermal Behavior of Ultra-fine Aluminium Powders (Alex)," *Proc. of the 29th Int. ICT Conf.*, 30 June – 3 July, Karlsruhe FRG, paper #30.
4. Ivanov G.V. and Tepper, F. (1996) "Activated Aluminium as a Stored Energy Source for Propellants," *Fourth Int. Symp. on Special Topics in Chemical Propulsion*, 27-28 May, Stockholm (Sweden), 636-44.
5. Miller P.J., Bedford C.D., and Davis J.J. (1998) "Effect of Metal Particle Size on the Detonation Properties of Various Metallised Explosives," *Proc. 11th Symp. (Intl.) on Detonation*, 31Aug – 4 Sep., Snowmass, CO., (ONR 33300-5) 214-20.
6. Cliff M.D., Dexter R.M. and Watt D.S. (2000) *The Effect of Ultrafine Electroexploded Aluminium (Alex) on Detonation Velocity and Pressure*, DSTO-TR-0999 (Limited Release).
7. Lefrancois A. and Le Gallic C. (2001) "Expertise [sic] of nanometric aluminium powder on the detonation efficiency of explosives," *Proc. of the 32th Int. ICT Conf.*, 3-6 July, Karlsruhe FRG, paper #36.
8. (a) Dorsett H.E., Brousseau P., and Cliff, M.D. (2001) "The influence of ultrafine aluminum upon explosives detonation," *28th Int. Pyrotech. Symp.*, 4-9 Nov 2001, Adelaide, South Australia; (b) Brousseau P., Dorsett H.E., Cliff M.D. and Anderson C.J. (2002) "Detonation properties of explosives containing nanometric aluminium powder," *Proc. 12th Symp. (Int.) on Detonation*, 11-16 Aug 2002, San Diego, CA.
9. (a) Cliff M.D., Dorsett H.E., and Lu J.-P. (2002) "Combustion of nanometric aluminium in detonating solid explosives," *The Usage and Performance of Nano-materials*, Feb-Mar 2002, Laurel, MD (USA); (b) Cliff M.D., Dorsett H.E., and Lu J.-P. (2002) "Combustion of nanometric aluminium in detonating solid explosives," *Symposium on New Materials III*, 2-4 April 2002, McLean, VA, USA.
10. Cooper P.W., *Explosives Engineering* (1996: Wiley-VCH, New York) 292.
11. Craig B.G., Johnson J.N., Mader C.L., and Lederman G.F. (1978) *Characterisation of Two Commercial Explosives*, (1978: Los Alamos Scientific Laboratory, New Mexico, USA) Technical Report LA-7140.
12. Goldstein S. and Johnson J.N. (1981) "Aquarium Tests on Aluminised ANFO," *Proc. of the 7th Symp. (Int.) on Detonation* (ONR, Annapolis MD), 1016-1023.

13. Dorsett H. and Katselis G. (1999) "Detonics modelling and Testing of IM (Insensitive Munition) Explosive," *PARARI'99 – 4th Aust. Exp. Ord. Symp.*, 10-13 Nov, Canberra (Australia).
14. (a) Brousseau P., Dorsett H.E., and Cliff M.D. (2002) "Nano-Particle Aluminum in Explosives," *29th Int. Pyrotech. Symp*., 14-19 July 2002, Westminster, Colorado USA; (b) Anderson C.J., and Katsabanis P. (2002) *Air-blast Measurements; Final Report*, from Mining Resource Engineering Limited, Kingston, Ontario, prepared for Defence Research Establishment Valcartier, Jan 2002.
15. Fickett W. and Davis W.C., *Detonation* (1979: Univ. of California Press: Berkeley).
16. Howe P., Frey R. and Melani G. (1976) "Observations Concerning Transverse Waves in Solid Explosives," *Comb. Sci. and Tech*. **14**, 63-74.
17. Chéret R., *Detonation of Condensed Explosives* (1993: Springer-Verlag, New York).
18. *See, for example,* Souers P.C. and Garza R. (1998), "Kinetic information from detonation front curvature," *Proc. 11th Symp. (Intl.) on Detonation*, 31 Aug –4 Sep., Snowmass, CO., (ONR 33300-5).
19. Ritter H. and Braun S. (2001) "High Explosives Containing Ultrafine Aluminum (ALEX)," *Propellants, Explosives, Pyrotechnics* **26**, 311-314.
20. Golgulya M.F., Dolgoborodov A.Yu., Brazhnikov M.A. and Baudin G., (1998) "Detonation waves in HMX/Al mixtures," *Proc. 11th Symp. (Intl.) on Detonation*, 31Aug – 4 Sep., Snowmass, CO., (ONR 33300-5).
21. Baudin G., Lefrançois A., Bergues D., Bigot J. and Champion Y. (1998) "Combustion of Nanophase Aluminium in the Detonation Products of Nitromethane," *Proc. 11th Symp. (Intl.) on Detonation*, 31Aug – 4 Sep., Snowmass, CO., (ONR 33300-5).
22. LeFrançois A., Baudin G., LeGallic C., Boyce P. and Coudoing J.-P. (2002) "Nanometric Aluminium powder influence on the detonation efficiency of explosives," *Proc. 12th Symp. (Int.) on Detonation*, 11-16 Aug 2002, San Diego, CA.
23. Tulis A.J., Sumida W.K., Dillon J., Comeyne W. and Heberlein D.C. (1998) "Submicron Aluminium Particle Size Influence on Detonation of Dispersed Fuel-Oxidizer Powders," *Arch. Comb.* **18**, 1-4, 157-164.
24. Maranda A., Cudzilo S., Trzciński W. and Nowaczewski J. (1998) "Behaviour of aluminium and TNT in the detonation wave of ammonium nitrate explosives", *Proc. of the 29th Int. ICT Conf.*, 30 June–3 July, Karlsruhe FRG, paper #43.
25. Brousseau P. and Cliff M.D. (2001) "The effect of ultrafine aluminium powder on the detonation properties of various explosives," *Proc. of the 32th Int. ICT Conf.*, 3-6 July, Karlsruhe FRG.
26. Cook M.A. (1957), *Jour. Phys. Chem*. **61**, 189-96.
27. Zerilli F., *ed*. (1981) *Notes on Detonation Physics*, NSWC MP 81-399.
28. Dremin A.N. *et al*. (1960) *DAN SSSR* **131**, 5, 1140-42.
29. *See, for example,* (a) Fox T.W., TeVelde J.A. and Nockolls J.A. (1976) "Shock wave ignition of metal powders," *Proc. Heat Transfer and Fluid Mech. Inst*., UC Davis, California, 241-256; (b) Veyssiere B. (1981) "Ignition of Aluminium Particles in a Gaseous Detonation," *8th ICOGER*, Minsk USSR Aug 23-26; (c) Afanas'eva E.A. and Levin V.A. (1987) "Aluminum particle ignition and combustion behind shock and detonation waves," *Combustion, Explosion and Shock Waves* **23**, 1, 8-14; (d) Bolobov V.I. (1994) "Mechanism of metal ignition in an oxygen flow," *Ibid*., **30**, 5, 29-33; *and*

(e) Boiko V.M. and Poplavskii S.V. (1999) "Ignition of aluminium powders mixed with liquid hydrocarbon fuels in air," *Ibid*., **35**, 1, 31-35.

30. *See, for example*, (a) Frost D.L., Zhang F., Murray S.B. and McCahan S. (2002) "Critical conditions for ignition of metal particles in a condensed explosive,", *Proc. 12th Symp. (Int.) on Detonation*, 11-16 Aug 2002, San Diego, CA.; (b) Goner A., Hooten I. and Narayan S. (2002) "Stead-state model of heterogeneous detonation with reactive metallic particles," *Ibid*.
31. Yang V., Brill T.B. and Ren W.-Z. *eds*., *Solid propellant chemistry, combustion and motor interior ballistics* (2000 Reston, Va.: Amer. Inst. of Aeronautics and Astronautics) 663-747.
32. (a) Davydov V. Yu, Grishkin A.M. and Feodoritov I.I. (1992) "Experimental-theoretical investigation of the oxidation of aluminium in detonation waves," *Combustion, Explosion and Shock Waves* **28**, 5, 124-128; (b) Bolobov V.I. (1998) "Mechanism of metal ignition in an oxygen flow," *Ibid*., **34**, 1, 44-50.
33. A. P. Il'in, A.A. Gromov, and G.V. Yablunovskii (2001) "Reactivity of Aluminum Powders," Combustion, Explosion and Shock Waves, 37, 4, pp 418-422.
34. Kury J.W., Breithaupt R.D. and Tarver C.M. (1999) "Detonation waves in Trinitrotoluene," *Shock Waves* **9**, 227-237.
35. Lubyantinsky S.N. and B.G. Loboiko B.G., (2002) "Detonation reaction zones in solid explosives," *Proc. 12th Symp. (Int.) on Detonation*, 11-16 Aug 2002, San Diego, CA.
36. Kato Y. and Brochet C. (1976), "Cellular structure of detonation in nitromethane containing aluminium particles," *Proc. 6th Symp. (Int.) on Detonation*, 24-27 Aug, Coronado, CA (Office of Naval Research ACR-221) 124-132.
37. Teychenne de Blazi P., Malaval C. and J.M. Lombard (1975) "Etude spectroscopique de la Température de Détoantion d'un Explosif contenant de l'Aluminium," Rapport final S75-01 CEG.
38. Lefrancois A., Grouffal J.-Y., Bouinot P. and Mencacci S. (2002) "Temperature and Pressure measurements comparison of the aluminised emulsion explosives detonation front and products expansion," *Proc. 12th Symp. (Int.) on Detonation*, 11-16 Aug 2002, San Diego, CA.
39. Leiper G.A. and Cooper J. (1998) "Reaction of aluminium and ammonium nitrate in non-ideal heterogeneous explosives," *Proc. 11th Symp. (Intl.) on Detonation*, 31Aug–4 Sep., Snowmass, CO., (ONR 33300-5).
40. Gogulya M.F., Dolgoborodov A. Yu, Makhov M.N., Brazhnikov M.A. and Shchetinin V.G. (2002) "Detonation performance of aluminised compositions based upon BNEN," *Proc. 12th Symp. (Int.) on Detonation*, 11-16 Aug 2002, San Diego, CA.
41. Sandstrom, F.W., Abernathy, R.L., Leone, M.G. and Banks, M.L. (1998) "Diameter effect, detonation front curvature and reaction rate modelling of ideal and non-ideal explosives," *28th DoD Explosives Safety Seminar*.

Appendix A: Image Analysis

A.1. Image interpretation

A.1.1 Frame images

A typical high-speed frame photograph from an aquarium test is shown in Fig. A1 below, with important features of the image labelled. These features include the detonation front (§ 3.2.1), the water shock and bubble profiles (§ 3.2.1 and § 3.2.3), and the angle of the water shock used to estimate the radial detonation pressure (§ 3.2.3.2).

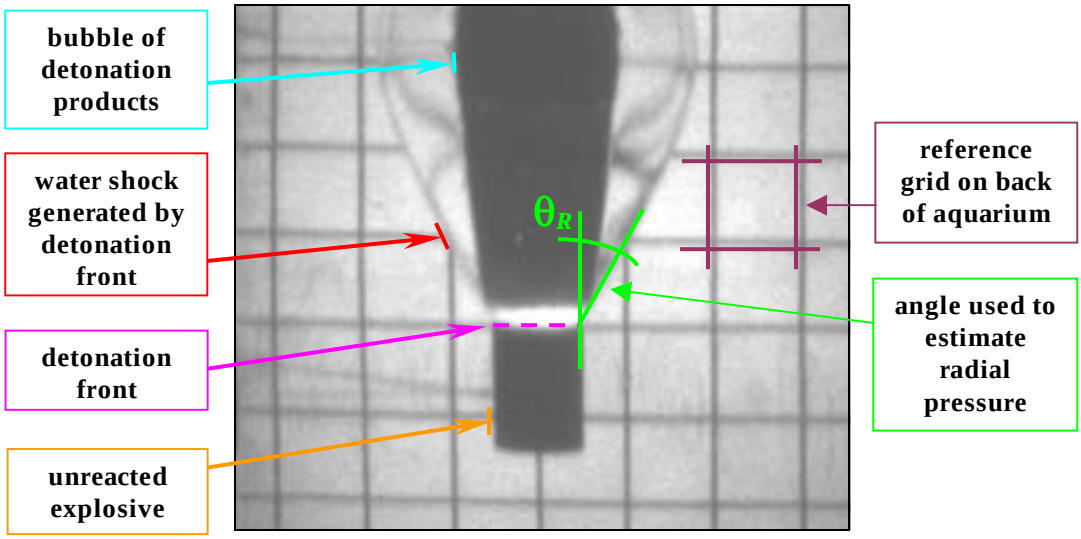

Figure A1. Frame photograph from aquarium test of a 2" charge of 'conventional' Tritonal made with Cap45a aluminium powder.

A.1.2 Streak images

Streak photographs are a one-dimensional, time-resolved record of an event, obtained by reducing the camera aperture to a slit along the direction of interest. For the aquarium tests, the slit was oriented along the centre axis of the charge, to record the progress of the detonation front from the one end of the charge (where the detonation is initiated) to the other. This is the general orientation for detonation velocity measurements. To measure detonation curvature, the slit was oriented across the bottom face of the charge to record the 'breakout' pattern of the detonation front.

A typical streak record of an aquarium test is shown in Fig. A2, along with a diagram of the slit orientation with respect to the charge and identification of salient features such as the detonation front and the light from the burning aluminium (§ 3.2.2). Also shown is the slope used to determine detonation velocities (§ 3.2.2.1) and the angle used to estimate detonation pressures (§ 3.2.2.2).

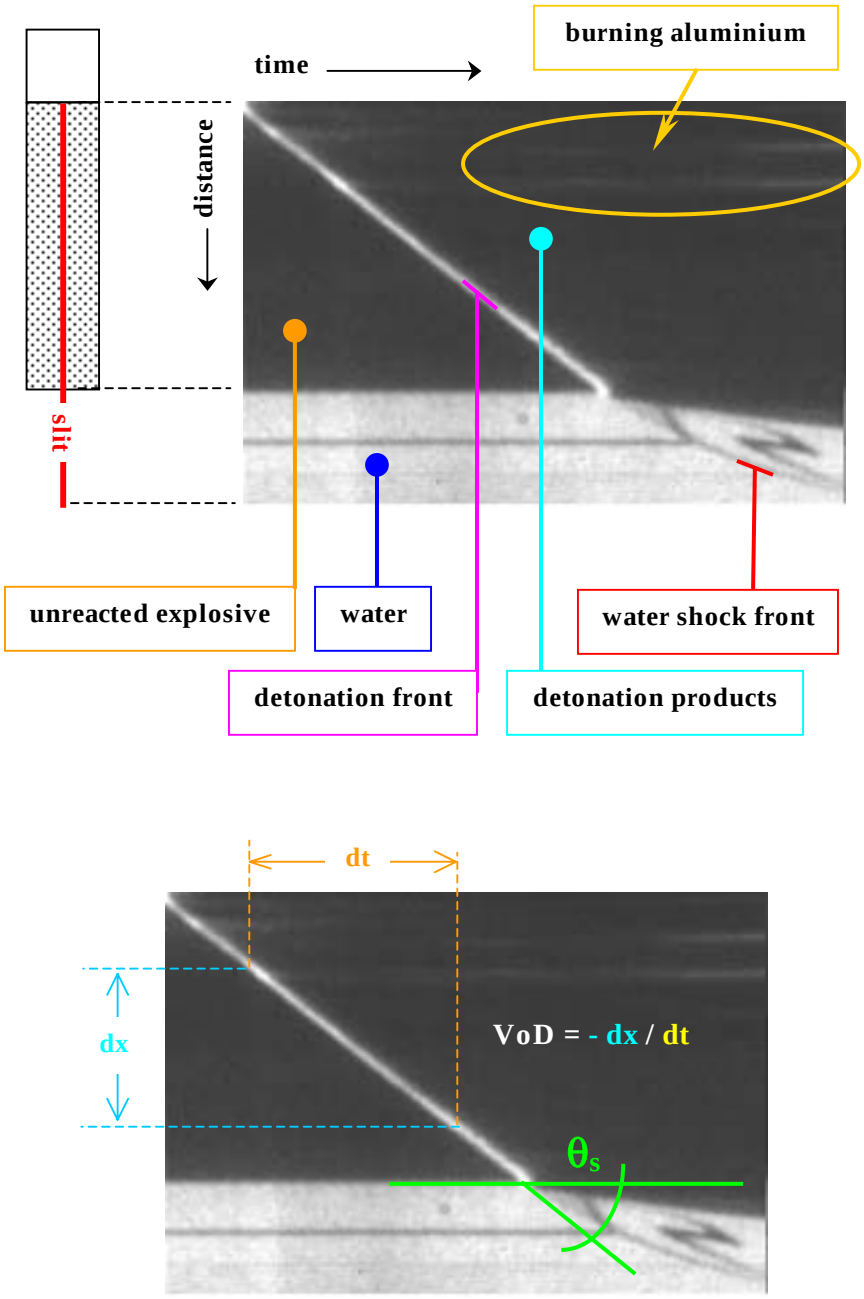

Figure A2. Top: streak image from aquarium test of a 2" diameter charge of 'conventional' Tritonal and diagram (left) showing alignment of camera slit (red line) with respect to the charge and booster. Bottom: same streak image illustrating the slope to obtain detonation velocity and the angle to determine detonation pressure.

A typical streak record of a detonation curvature measurement is shown in Fig. A3, along with diagrams of the experimental setup to illustrate the relationship between the spatial curvature of the detonation front and the 'temporal' curvature recorded by the slit camera.

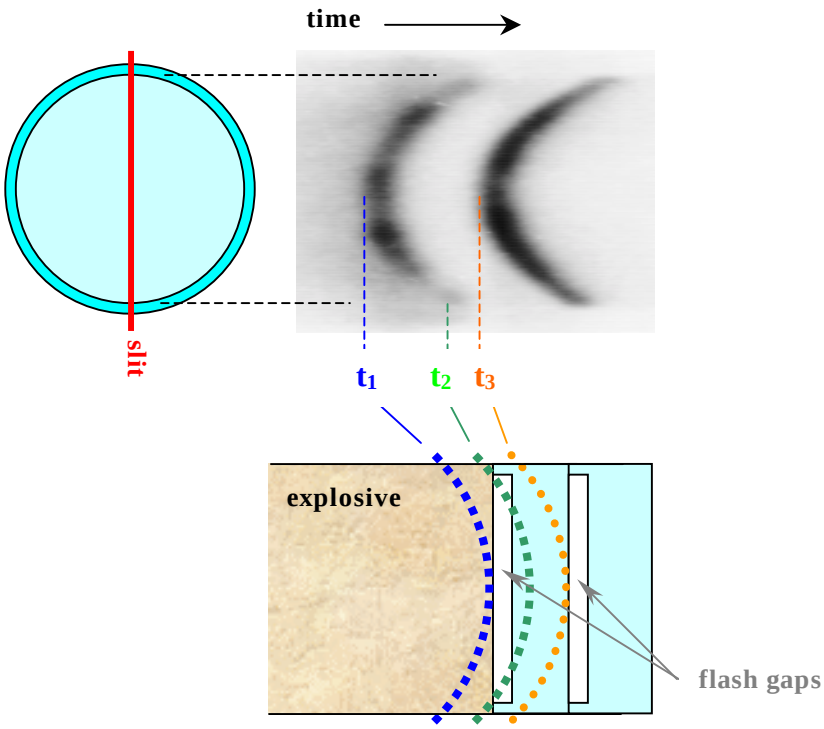

Figure A3. Top: (right) streak image from detonation front curvature measurement of a failing detonation in a 1" diameter charge of TNT and (left) diagram showing alignment of camera slit with respect to end of charge. Bottom: diagram of the end of the charge with the two Perspex flash gaps, showing positions of the detonation shock front (dashed curves) at three different times with respect to their traces on the streak record. To enhance features of the streak record, the grey scale has been inverted (i.e., the photographic 'negative' is shown).

A.2. Image calibration

The tables below give relevant information for calibrating CCD images taken for the aquarium tests and the flash gap measurements of detonation front curvature. In this report, length scales were derived from the lengths of the charges in "static" photographs taken before the experiment, and time scales were obtained from the writing speed of the streak camera. The event number serves as an index for the images stored on the accompanying CD-ROM.

Table A1. Length and time scales for calibration of aquarium test images.

Explosive	No.	l_{exp} [a] (mm)	Δt_{str} [b] (μs)	Timings of frame photographs (microseconds) [c] 1	2	3	4	5	6	7
1" (25.4mm) TNT/Cap45a	**1**	200.4	60	15.11	24.34	30.49	36.64	50.	66.	82.
	11	200.4	60	18.18	24.34	30.49	36.64	50.	66.	82.
	12	200.3	100	24.34	36.64	42.	58.	74.	87.	100.
1" (25.4mm) TNT/Alex®	**2**	199.6	60	15.11	24.34	30.49	36.64	50.	66.	82.
	13	194	60	16.33	22.3	28.27	34.24	50.	66.	82.
	14	184	100	17.	22.	27.	32.	45.	58	74.
2" (50.8mm) TNT/Cap45a	**3**	200.05	60	18.38	24.53	30.68	36.83	50.	66.	82.
	7	199.9	60	18.38	24.53	30.68	36.83	50.	66.	82.
	8	199.9	100	*Back-lighting failure – no imaging of the water shock.*						
2" (50.8mm) TNT/Alex®	**4**	199.9	60	18.38	24.53	30.68	36.83	50.	66.	82.
	5	195	60	18.38	24.53	30.68	36.83	50.	66.	82.
	6	199.8	60	18.38	22.97	27.56	32.15	50	36.74	41.33
2" (50.8mm) TNT	**9**	200	60	17.97	23.86	29.74	35.62	48.5	64.5	80.5
	10	200	60	17.97	23.86	29.74	35.62	48.5	64.5	80.5

[a] The length of the explosive charge. [b] The duration of the streak measurement.
[c] All timings have a precision of ± 0.001 microseconds.

Table A2. Length and time scales for calibration of detonation front curvature images.

Explosive	No.	Δt_{str} [a] (μs)	disk [b] thickness (mm)	gap thickness (microns)	VoD (mm/μs)	Comments
1" (25.4mm) TNT/Cap45a	**18**	8	2.3	500	6.771	R_d ~ 60mm
	26	6	2.24	100	6.714	R_d ~ 140mm
	27	6	2.25	100	6.772	
1" (25.4mm) TNT/Alex®	**19**	8	2.45	500	6.762	oddly-shaped front
	25	6	2.72	100	6.752	
	28	6	2.45	100	6.814	
2" (50.8mm) TNT/Cap45a	**16**	8	2.55	250	6.859	R_d ~ 320mm
	17	6	2.55	500	6.717	anomalous curv.
	22	6	2.4	250	6.968	R_d ~ 320mm
2" (50.8mm) TNT/Alex®	**21**	6	2.4	250	6.811	oddly-shaped front
	23	6	2.4	250	6.807	
	24	6	2.4	250	6.834	
1" (25.4mm) TNT	**20**	8	--	--	4.894	missed signal
	29	16	2.5	100	4.762	R_d ~ 140mm
	30	16	--	--	*failure*	missed signal

[a] Duration of the streak measurement. [b] Thickness of the first Perspex disk

Appendix B: Derivation of Pressure Equations

B.1. Detonation pressure

The detonation (or CJ) pressure of the explosive is estimated from the shock profile produced in the water produced by the detonation by assuming that the magnitude of the pressure does not change as the detonation front enters the water from the end of the explosive

$$P_{CJ} = P_S . \qquad \text{(B1)}$$

The velocity of the water shock U_S is obtained from the streak record by determining the slope dx/dt of the water shock profile at the point the shock exits the charge.

$$U_S = dx/dt \qquad \text{(B2)}$$

The relationship between the pressure and velocity of a shock wave is obtained from conservation of momentum

$$P_S - P_0 = \rho_0 U_S U_p , \qquad \text{(B3)}$$

where U_s is the velocity of particle motion, and P_0 is the initial pressure. Since for aquarium tests, the initial pressure is one atmosphere - approximately six orders of magnitude smaller than the shock pressures - P_0 is set to zero:

$$P_S = \rho_0 U_S U_p . \qquad \text{(B4)}$$

For shocked materials, the relationship between shock velocity and particle velocity can be described fairly well by a linear equation[13]

$$U_S = C_0 + s U_p , \qquad \text{(B5)}$$

Where C_0 is the sound velocity in the material at zero pressure, and s is an empirical parameter obtained by fitting experimental data. Combining equations B1, B4 and B5 gives the relationship for estimating shock pressure:

$$P_{CJ} = P_S = U_S \rho_0 (U_S - C_0) / s . \qquad \text{(1)}$$

B.2. Radial pressure

As with detonation pressure, the radial pressure is estimated by assuming the pressure is constant across the explosive-water interface, and can be estimated from the radial velocity of the shock front in the water:

$$P_R = P_{S,R} = U_{S,R} \rho_0 (U_{S,R} - C_0) / s . \qquad \text{(B6)}$$

For frame photographs, the velocity of the water shock must be estimated from the known velocity of the detonation front within the explosive. This is achieved by measuring the angle of the water shock with respect to the motion of the detonation front.

[13] This relationship assumes the material does not undergo a phase transition.

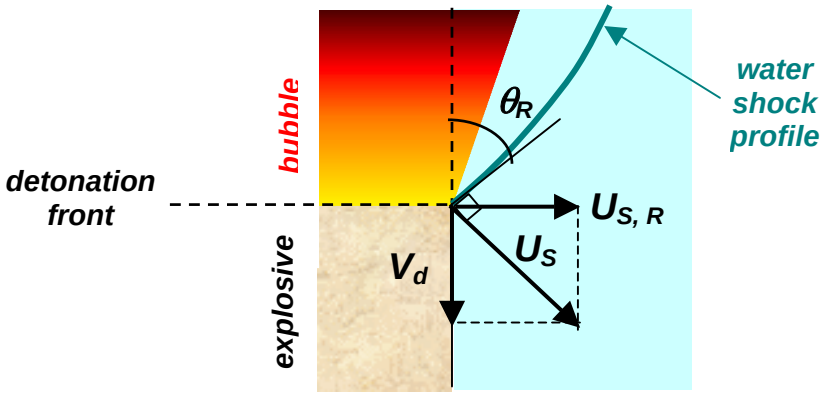

Figure B1. Vector diagram of detonation and water shock velocities.

The velocity of the water shock is normal to the surface of the shock profile, and at the point the shock exits the surface of the charge, may be expressed as a vector sum of the detonation velocity and radial shock velocity:

$$\vec{U}_S = \vec{U}_{S,R} + \vec{V}_d \qquad \text{(B7)}$$

By geometry, the angle of the shock velocity vector $\vec{U}_S$ with respect to the edge of the charge (and to the detonation velocity $\vec{V}_d$) is equal to the angle θ_R between the shock profile and the edge of the charge. The scalar magnitudes of the velocities are then

$$V_d = U_S \cos \theta_R \qquad \text{(B8)}$$

and

$$U_{S,R} = U_S \sin \theta_R \ . \qquad \text{(B9)}$$

Combining equations B8 and B9 gives the relationship between the detonation velocity and the radial shock velocity

$$U_{S,R} = V_d \tan \theta_R \ . \qquad \text{(B10)}$$

Substituting this expression for the radial shock velocity into Eq. B6 gives the relationship

$$P_R = V_d \tan \theta_R \ \rho_0 (V_d \tan \theta_R - C_0) / s \ . \qquad (2)$$

DISTRIBUTION LIST

Detonation Front Curvature Measurements and Aquarium Tests of Tritonal Variants

Helen E. Dorsett and Matthew D. Cliff

AUSTRALIA

DEFENCE ORGANISATION

Task Sponsor

Joint Ammunition and Logistics Organisation
Defence Establishment Orchard Hills, Sydney, NSW 2784
WGCDR Wade Evans
LEUT Michael McGrann

S&T Program

Chief Defence Scientist
FAS Science Policy
AS Science Corporate Management
Director General Science Policy Development
} shared copy

Counsellor Defence Science, London (Doc Data Sheet only)
Counsellor Defence Science, Washington (Doc Data Sheet only)
Scientific Adviser to MRDC Thailand (Doc Data Sheet only)
Scientific Adviser Joint
Navy Scientific Adviser (Doc Data Sheet and Distribution List only)
Scientific Adviser - Army (Doc Data Sheet and Distribution List only)
Air Force Scientific Adviser (Doc Data Sheet and Distribution List only)
Scientific Adviser to the DMO (Doc Data Sheet and Distribution List only)
Director of Trials

Systems Sciences Laboratory

Chief, Weapons Systems Division (Doc Data Sheet and Distribution Sheet Only)
Research Leader: Dr. Norbert Burman, WSD Edinburgh
Task Manager: Dr. Matthew D. Cliff, SO LHQ, Sydney
Author: Dr. Helen Dorsett, MOD Pyrmont (3 copies)

Dr. William S. Wilson
Dr. Jing-Ping Lu
Dr. Anna Wildegger-Gaissmeyer
Dr. Jeremy Anderson
Dr. George Katselis
Mr. Carmine Caputo
Mr. David Fraser

DSTO Library and Archives

Library Edinburgh 1 copy and Doc Data Sheet
Australian Archives

Capability Systems Division

Director General Maritime Development (Doc Data Sheet only)
Director General Land Development
Director General Aerospace Development (Doc Data Sheet only)
Director General Information Capability Development (Doc Data Sheet only)

Office of the Chief Information Officer

Chief Information Officer (Doc Data Sheet only)
Deputy CIO (Doc Data Sheet only)
Director General Information Policy and Plans (Doc Data Sheet only)
AS Information Structures and Futures (Doc Data Sheet only)
AS Information Architecture and Management (Doc Data Sheet only)
Director General Australian Defence Information Office (Doc Data Sheet only)
Director General Australian Defence Simulation Office (Doc Data Sheet only)

Strategy Group

Director General Military Strategy (Doc Data Sheet only)
Director General Preparedness (Doc Data Sheet only)

HQAST

SO (ASJIC) (Doc Data Sheet only)

Navy

SO (SCIENCE), COMAUSNAVSURFGRP, NSW (Doc Data Sheet and distribution list only)

Army

ABCA National Standardisation Officer, Land Warfare Development Sector, Puckapunyal (4 copies)
SO (Science), Deployable Joint Force Headquarters (DJFHQ) (L), Enoggera QLD (Doc Data Sheet only)
SO (Science) - Land Headquarters (LHQ), Victoria Barracks NSW (Doc Data Sheet and Executive Summary Only)
NPOC QWG Engineer NBCD Combat Development Wing, Puckapunyal, VIC (Doc Data Sheet relating to NBCD matters only)

Air Force

Director General Policy and Plans, Air Force Headquarters (Doc Data Sheet only)
Director General Technical Air Worthiness, RAAF Williams (Doc Data Sheet only)
Chief of Staff – Headquarters Air Command, RAAF Glenbrook (Doc Data Sheet only)
Commander Aircraft Research and Development Unit, RAAF Edinburgh (Doc Data Sheet only)
Commander Air Combat Group, RAAF Williamtown (Doc Data Sheet only)
Staff Officer (Science), RAAF Amberley (Doc Data Sheet only)
Staff Officer (Science), RAAF Williamtown (Doc Data Sheet only)
Commander Air Lift Group, RAAF Richmond (Doc Data Sheet only)
Commander Maritime Patrol Group, RAAF Edinburgh (Doc Data Sheet only)
Commander Surveillance Control Group, RAAF Williamtown (Doc Data Sheet only)

Commander Combat Support Group, RAAF Amberley (Doc Data Sheet only)
Commander Training, RAAF Williams (Doc Data Sheet only)

Intelligence Program

DGSTA Defence Intelligence Organisation
Manager, Information Centre, Defence Intelligence Organisation
Assistant Secretary Corporate, Defence Imagery and Geospatial Organisation (Doc Data Sheet only)

Defence Materiel Organisation

Head Airborne Surveillance and Control (Doc Data Sheet only)
Head Aerospace Systems Division (Doc Data Sheet only)
Head Electronic Systems Division (Doc Data Sheet only)
Head Maritime Systems Division (Doc Data Sheet only)
Head Land Systems Division (Doc Data Sheet only)

Defence Libraries

Library Manager, DLS-Canberra (Doc Data Sheet Only)
Library Manager, DLS - Sydney West (Doc Data Sheet Only)

UNIVERSITIES AND COLLEGES

Australian Defence Force Academy
Library
Head of Aerospace and Mechanical Engineering
Serials Section (M list), Deakin University Library, Geelong, VIC
Hargrave Library, Monash University (Doc Data Sheet only)
Librarian, Flinders University

OTHER ORGANISATIONS

National Library of Australia
NASA (Canberra)
State Library of South Australia

OUTSIDE AUSTRALIA

INTERNATIONAL DEFENCE INFORMATION CENTRES

US Defense Technical Information Center, 2 copies
UK Defence Research Information Centre, 2 copies
Canada Defence Scientific Information Service, 1 copy
NZ Defence Information Centre, 1 copy

ABSTRACTING AND INFORMATION ORGANISATIONS

Library, Chemical Abstracts Reference Service
Engineering Societies Library, US
Materials Information, Cambridge Scientific Abstracts, US
Documents Librarian, The Center for Research Libraries, US

INFORMATION EXCHANGE AGREEMENT PARTNERS

Acquisitions Unit, Science Reference and Information Service, UK

Defence Research Establishment, Valcartier
2459 Pie-XI Blvd North, Val-Belair, QC, G3J 1X5, Canada
Mr. Patrick Brousseau

SPARES (5 copies)

Total number of copies: **48**

DEFENCE SCIENCE AND TECHNOLOGY ORGANISATION
DOCUMENT CONTROL DATA

1. PRIVACY MARKING / CAVEAT (OF DOCUMENT)

2. TITLE

Detonation Front Curvature Measurements and Aquarium Tests of Tritonal Variants

3. SECURITY CLASSIFICATION (FOR UNCLASSIFIED REPORTS THAT ARE LIMITED RELEASE USE (L) NEXT TO DOCUMENT CLASSIFICATION)

Document	(U)
Title	(U)
Abstract	(U)

4. AUTHOR(S)

Helen Dorsett and Matthew D. Cliff

5. CORPORATE AUTHOR

Systems Sciences Laboratory
PO Box 1500
Edinburgh South Australia 5111 Australia

6a. DSTO NUMBER	6b. AR NUMBER	6c. TYPE OF REPORT	7. DOCUMENT DATE
DSTO-TR-1411	AR-012-729	Technical Report	April 2003

8. FILE NUMBER	9. TASK NUMBER	10. TASK SPONSOR	11. NO. OF PAGES	12. NO. OF REFERENCES
9505 / 23 / 220	JNT 01 / 221	JALO	37	41

13. URL on the World Wide

http: / / www.dsto.defence.gov.au / corporate / reports / DSTO-TR-1411.pdf

14. RELEASE AUTHORITY

Chief, Weapons Systems Division

15. SECONDARY RELEASE STATEMENT OF THIS DOCUMENT

Approved for public release

OVERSEAS ENQUIRIES OUTSIDE STATED LIMITATIONS SHOULD BE REFERRED THROUGH DOCUMENT EXCHANGE, PO BOX 1500, EDINBURGH, SA 5111

16. DELIBERATE ANNOUNCEMENT

No Limitations

17. CITATION IN OTHER DOCUMENTS Yes

18. DEFTEST DESCRIPTORS

Aluminised explosives, trinitrotoluene, Tritonal, detonation

19. ABSTRACT

'Alex', an ultrafine aluminium powder, burns more rapidly than conventional aluminium powders in energetic materials. In TNT-based formulations, the increased rate of energy release leads to higher detonation pressures and velocities. In order to determine the rate of Alex combustion in solid explosives, and to further assess its effects on the detonation properties of TNT formulations, aquarium tests and detonation front curvature tests were performed on Tritonal variants. The aquarium tests definitively show that Alex combustion in detonating Tritonal is significantly faster than that of Cap45a, the conventional aluminium powder used for military explosives. Additional pressure and velocity measurements from the aquarium tests agree with previous experiments. The results of detonation front measurements were less conclusive, but show qualitive trends that support existing data.